SONJA SCHMID

THE EFFECT OF PHOSPHORYLATION ON SUBSTRATE BINDING OF THE SMALL HEAT-SHOCK PROTEIN αB-CRYSTALLIN

THE EFFECT OF PHOSPHORYLATION ON SUBSTRATE BINDING OF THE SMALL HEAT-SHOCK PROTEIN αB-CRYSTALLIN

SONJA SCHMID

Master Thesis

Nanoscience Curriculum
Philosophisch-Naturwissenschaftliche Fakultät
Universität Basel

April 2010

Dedicated to the best man walking:
Thomas Post, my constant support & inspiration.

ABSTRACT

Herein, we present a study on the small heat-shock protein (sHsp) and human eye lens protein αB-crystallin (αB) regarding its substrate binding capabilities, the effect of post-translational phosphorylation at residues 19, 45 and 59, and the interplay with supplementary chaperones.

To this end, phospho-mimetic αB mutants were cloned, wild-type and mutants were recombinantly expressed in *e.coli*, and purified. Analysis with HPLC and analytical ultra-centrifugation (AUC) revealed 24-meric oligomers for wild-type αB-crystallin, but smaller 12 - 16-mers for the phospho-mimic. Applying the same analytical techniques, binding of the model substrate, malate dehydrogenase (MDH), was only observed with the phospho-mimetic form of αB where a broad distribution of substrate complexes with varied stoichiometries was found. Additionally, in aggregation assays based on unfolding due to heat *or* acidic conditions, phospho-mimetic αB showed increased chaperone activity as compared to the wild-type. Moreover, refolding assays together with the human Hsp70/Hsp40 - system revealed five times better substrate recovery, when preceded by substrate deactivation in the presence of the phospho-mimic as against to wild-type αB.

We conclude that phosphorylation of αB leads to an oligomeric species with amplified reactivity towards MDH. Therefore, a constant high level of phosphorylated αB *in vivo* may be pathogenic in terms of a gain of function.

ZUSAMMENFASSUNG - SUMMARY IN GERMAN FOR THE NON-SCIENTIFIC READER

Proteine sind die molekularen Maschinen - *die Macher* - der biologischen Zelle. Weil sie an allen Prozessen im Zellalltag als Enzyme oder Strukturelemente beteiligt sind, sind sie für die Zelle unerlässlich. Dies widerspiegelt sich schon im Namen, der 1838 von Jöns Jakob Berzelius vorgeschlagen wurde: πρωτεῖοσ also *proteios* ist griechisch für grundlegend.

Ausserdem sind Proteine aufwändig in der Herstellung. Jedes einzelne Protein wird genau nach seinem Bauplan, der als Gen im Zellkern gespeichert ist, nachgebaut. Das Ribosom - auch ein Protein - liest diese Information im Zellplasma von einer Kopie des entsprechenden Genes ab und hängt Schritt für Schritt die vorgeschriebenen Aminosäuren aneinander. Das Resultat ist eine Kette von Aminosäuren, ein so genanntes Peptid, das sich genau in *eine* zweckmässige Struktur falten kann und muss, damit es seine Funktion ausüben kann.

Das Finden der richtigen 3-dimensionalen Struktur ist aber gar nicht so einfach, z.B. weil es im Innern der Zelle nicht ausreichend Platz gibt, damit sich die neuen Proteine erst einmal ganz ausstrecken könnten. Im Gegenteil, alles ist voll mit anderen Proteinen, aber auch Zucker-Verbindungen und Fetten. Und was es in diesem überfüllten Raum zu verhindern gilt, ist das unkontrollierte Zusammenkleben der Proteine in grossen Klumpen. Deshalb ist im Verlauf der Evolution eine neue Klasse an Helfer-Proteinen entstanden: die Chaperone (engl./franz. für Anstandsdame).

Die Aufgabe dieser Chaperone ist es, den neu gebauten Aminosäure-Ketten erstmal in ihre angestammte Form zu helfen. Schliesslich sind sie nur so ein richtiges Protein und können ihre Aufgabe in der Zelle erfüllen. Es kann aber auch sein, dass funktionstüchtige Proteine ihre Gestalt wieder verlieren. Dies kommt sehr häufig vor wenn es im Umfeld der Zelle heiss wird. Dass die Zelle dann nicht zu einem einzigen Spiegelei wird, also alles verklumpt oder aggregiert, darauf haben sich die *kleinen Hitze-Schock Proteine* (sHsp), eine Untergruppe der Chaperone, spezialisiert. Sie halten die einzelnen Proteine fest sobald diese zum Verklumpen tendieren. Weil es dadurch nicht zu einem riesigen Aggregat kommt, sondern die gebundenen Proteine (Substrate) separat in Lösung bleiben, können sie später wieder reaktiviert werden.

Gerade in unserer Augenlinse sind solche Prozesse extrem wichtig, damit sich kein Grauer Star entwickelt. Auch andere auf Aggregation basierende Krankheiten wie Alzheimer, Parkinson und Creutzfeldt-Jakob werden mit sHsps assoziiert. Das kleine Hitze-Schock Protein, welches im Auge - aber auch andernorts - die Aggregation unterdrückt, heisst α*B-crystallin*. In dieser Master-Thesis wurde die Substratbindung dieses αB-crystallins (αB) untersucht.

Neben der Originalversion des αB wurde auch noch eine zweite Art, die an drei Stellen modifiziert ist, so wie es in der Zelle auch vorkommt, einbezogen. Es zeigte sich, dass die modifizierte Form (in unserem Fall ist sie *phosphoryliert*), die Aggregation des Substrats besser unterdrücken kann.

Diese kleinen Hitze-Schock Proteine agieren meistens in grossen Verbänden. Ein Komplex der Originalversion von αB enthält 24 Untereinheiten, wohingegen die phosphorylierte Version kleinere Komplexe à 12 - 16 Untereinheiten bildet. Die Bindung von Substrat-Proteinen allerdings konnte nur für die phosphorylierte αB Form wirklich nachgewiesen werden. Hier wurde eine breite Verteilung verschieden grosser αB-Substrat-Komplexe gefunden. Die zeitweilig inaktiven Substratproteine dieser Komplexe konnten schliesslich mit der Hilfe anderer Chaperone auch wieder reaktiviert werden. Allerdings nur ein kleiner Teil, aber auch hier zeigte

sich das phosphorylierte αB als potenteres Mittel. Es könnte also sein, dass sich die Zelle mit diesem modifizierten αB während Stress-Situationen zusätzlich schützt. Wenn diese offensichtlich reaktivere Form aber dauerhaft auftritt, könnte sie auch pathogene Folgen haben, in dem sie beispielsweise *intakte* Proteine bindet.

CONTENTS

LIST OF FIGURES

1 INTRODUCTION

A biological cell is a very crowded place: many organelles, the cytoskeleton and countless other substances such as nucleic acids, sugars, fats and proteins gather in a viscous cytoplasm. In this environment, new proteins are synthesized by ribosomes which translate the genetic code into a sequence of amino acids.

This, however, is not a useful protein, yet. Correct folding of the primary sequence is required for a fully functional protein. Thereby, each amino-acid sequence encodes for a 3-dimensional structure, which is conditional for proper protein function. Immersed in this over-populated media, correct folding is not an easy task to do. Yet, the stakes are high when it comes to protein folding, since the cell depends largely on these molecular machines.

Therefore, a sophisticated refolding machinery has evolved which assists proteins in this critical operation: the chaperones. The name of this group of proteins relates to their duty to help young species to find their mature shape and to keep them away from bad interactions.

This is an accurate summary of the role of molecular chaperones in the cytosol and several cellular compartments. Chaperones interact with newly synthesized proteins that have there hydrophobic residues not yet hidden from the hydrophilic surrounding [16][17]. By this, they prevent unspecific (co-)aggregation with other newly synthesized proteins, degraded proteins or with them-selves. In this context, a controlled substrate release distinguishes the chaperone from any other interaction partner.

Further chaperones exert force on their substrate in order to push and pull it into its native fold. Others simply offer the substrate some empty, water-free space that allows it to reach its proper structure. Moreover, chaperones are related to controlled protein unfolding and disintegration of existing aggregates to keep the cell free from such debris [18][4]. Because many chaperones are expressed at increased levels during stress situations including heat stress, they are alternatively called heat-shock proteins (Hsps) [19].

Knowing the diverse duties of the chaperone family, it is no surprise that nature invented many different chaperone structures - each optimized for the respective function. Figure 1 includes only a small selection of the most prominent chaperones.

The chaperonins constitute the best studied class of chaperones. They are huge in size as indicated in Figure 1a where the 1 MDa GroEL/GroES complex from *E.coli* is displayed. The shape of this Hsp60/Hsp10 complex resembles a barrel built from a trans-(red) and cis-ring (green), each composed of 7 GroEL units (Hsp60), and capped by the GroES lid (Hsp10, orange) [17]. The GroEL/GroES mechanism includes packing of a partially unfolded substrate into the inside of the barrel, ATP dependent lid closure, and simultaneous conformational rearrangements (cf. asymmetry of *cis* and *trans* ring in the illustration). As a consequence, the substrate is set free within the cavity, and - in the absence of further interaction partners - it possibly finds its native fold [20].

In contrast to the large, multi-meric chaperonin complexes, Hsp90 adopts a dimeric structure. Its chaperone mechanism, however, is by far more complex and less understood. This although, it is known that many important enzymes, especially kinases, crucially depend on the chaperone activity of Hsp90 [17]. Many cofactors and interaction partners have been identified so far. Among those p23 which is associated to the closed form of Hsp90 displayed in Figure 1b [21].

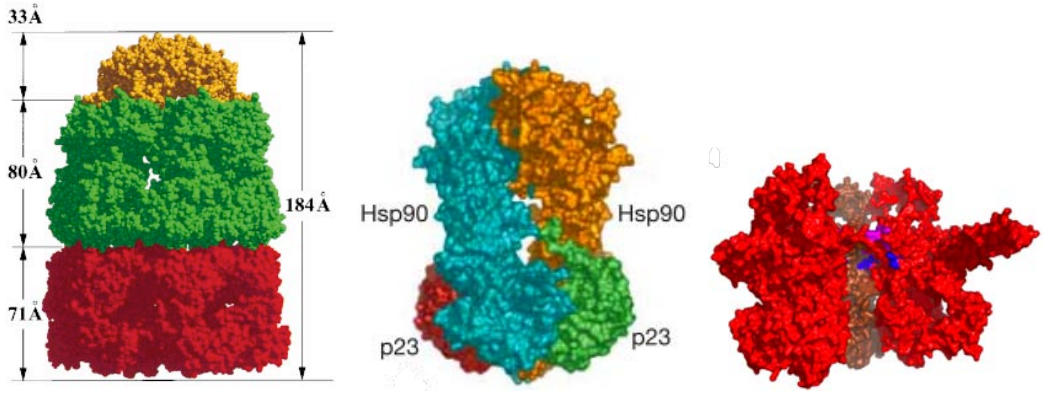

(a) (b) (c)

Figure 1: Representatives of three chaperone categories: (a) the chaperonin complex GroEL/GroES from *Escherichia coli* [1]. (b) Closed form of the Hsp90 dimer from *Saccharomyces cerevisiae* with bound cofactor p23 [2]. (c) The Hsp100 representative, ClpB from *Thermus thermophilus*. Only four of the six subunits are drawn in order to display the central channel. The residues in blue and pink are part of the *diaphragm* involved in polypeptide translocation (originally from [3], retrieved from [4]).

Additionally, Hsp90 can adopt an open conformation, too, where the N-terminal domains (top domains in the illustration) are shifted sideways. The corresponding conformational changes were associated with activation or deactivation of particular substrates [21]. But the origin of these conformational changes within the chaperone mechanism is not completely understood, yet. Though, it was shown that conformational fluctuations much faster than Hsp90's ATPase rate are involved [22].

The third illustration in Figure 1 represents the Hsp100 chaperone category. Hexameric ClpB, a caseinolytic peptidase B protein homolog from *T. thermophilus*, is displayed. This chaperone deals mostly with polypeptides whose biosynthesis has failed. Together with other chaperone associates, it is capable of decomposing stable protein aggregates [4]. A mechanistic model suggests that the bound substrate is threaded through the central channel of ClpB under continuous ATP hydrolysis by two AAA+ modules [3]. Thus, unfolding is stimulated and the substrate protein is either directed to the degradation machinery or towards refolding under assistance of Hsp70.

After this opening survey of three model chaperones, it is easy to imagine what happens if some chaperone activities are impaired: hampered protein folding, increased aggregate levels are the consequences. Diseases due to loss *or* gain of function may arise. An example of the latter was found in yeast, where prion formation critically depends on Hsp104 [23]. Furthermore, chaperones including Hsp90 are becoming drug targets in cancer therapy [24]. And the small heat-shock proteins, introduced in the next section, are related to cataract, many aggregation associated neurodegenerative diseases [25] and myopathies [26]. These severe diseases should be a good reason for getting a closer look at this influential molecular machines.

1.1 THE SMALL HEAT-SHOCK PROTEIN αB-CRYSTALLIN

In contrast to the chaperone families presented above, small heat-shock proteins (sHsps) operate in an ATP independent way [27]. They are evolutionary very wide-spread and have been found in all three taxonomical domains, with increased specie numbers in higher eukaryotes [6].

As the name implies, a common feature of sHsps is their comparably small size (12 - 40 kDa [5], typically about 20 kDa) and their elevated expression levels during stress periods caused by heat but also by many other types of stress including acidic conditions [28], exposure to toxins like ethanol, arsenic, trace metals, ultraviolet light, as well as infection, inflammation, exercise, starvation, water or oxygen deprivation, and nitrogen deficiency in plants [29].

During periods of stress, sHsps exert anti-aggregating capabilities. Partially unfolded proteins are bound by hydrophobic interactions with denatured stretches of the respective protein. Thereby, the substrate is kept soluble and its aggregation is suppressed. On the other hand, sHsps lack the ability to initiate refolding of their substrates on their own. Consequently, additional chaperones, such as those discussed above, are required to assist refolding of the partially unfolded, but solubilized substrates [30]. Thus, sHsps operate as a buffer that binds aggregation prone candidates during stress periods, keeps them in a refolding-competent state and releases them again when deleterious conditions are terminated, and/or a chaperone is ready to assist new assembly [31].

In addition, sHsps are involved in actin polymerization, regulation of cellular redox states and negative regulation of apoptosis [25]. The relevance of these chaperone category is best demonstrated by the fact that organisms lacking sHsps develop severe disorders. In the case of αA-crystallin knock-out mice, early cataract along with inclusion bodies containing αB-crystallin was reported [32]. Moreover, general sensitivity to heat was found in Hsp16.6 deficient cyanobacteria [33].

The most prominent representatives among sHsps are the previousely mentioned α-crystallins. Toghether with the β- and γ-crystallins they comprise the major protein components in the lens of vertebrate eyes [34], which also led to their name. They are the source of the lens' transparency which is achieved by very dense, liquid crystal-type packing of the crystallin proteins, resulting in a high refractive index. In this regard, the α-crystallins are in charge of preserving this crystallinity a life long - without any protein replacement, nota bene [35][25]. This makes α-crystallins particularly special.

One of the two known isoforms is αB-crystallin (HSPB5, SwissProt entry: P02511), whose human representation was studied herein (subsequently referred to as αB). As compared to its homologue αA-crystallin, αB is more appealing, because of its occurrence in many tissues all over the human body: this 20 kDa protein is not only present in the lens, but also in the brain, lung, cardiac and skeletal muscle [36]. Whereas the main substrates in the eye lens are β- and γ-crystallins, αB was shown to bind *in vitro* many other substrates including β-crystallin, luciferase, malate and lactate dehydrogenase, T4 lysozyme, citrate synthase, insulin, the Parkinson's disease related α-synuclein, actin and desmin [28][37].

This reflects the promiscuous attitude of sHsps: hydrophobic interactions allow to bind any hydro-phobic residues that are turned to the outside, in a very unspecific way. Therefore, knowledge about the actual binding site is quite limited and contradictory statements about involvement of the α-crystallin domain, as well as the N- or C-terminal domain have been published [38][39]. Newer results about peptides involved in binding indicate that such general domain assignment is not applicable [40]. Rather it seems that interaction sites vary with substrates and experimental conditions, such as temperature [41]. The existence of a specific

recognition sequence, by which potential substrates are identified, is rather improbable, because of the unspecific binding interaction.

Additionally to common function, *structural* homology is found within the genetically diverse class of sHsps: the conserved α-crystallin domain is located close to the C-terminus of the sHsps. This 80 - 100 residue domain is named after the eponymous eye lens protein, α-crystallin. It includes predominantly β-strands as shown in Figure 2. The α-crystallin domain is flanked by a relatively variable N-terminal domain and a short C-terminal extension [6][5].

As illustrated by Figure 2(c), the α-crystallin domain adopts a β-sandwich fold familiar to immunoglobulins. Subunit interactions involving the α-crystallin domain together with the N-terminal domain give rise to dimerization. In the most cases, the dimer is stabilized by the α-crystallin domain (cf. swapped β-strands in the illustration) and the N-terminal domain. On the other hand, the N- and C-terminal domains are associated with oligomer formation, where dimers are thought to constitute the basic building blocks (see Figure 2(b)).

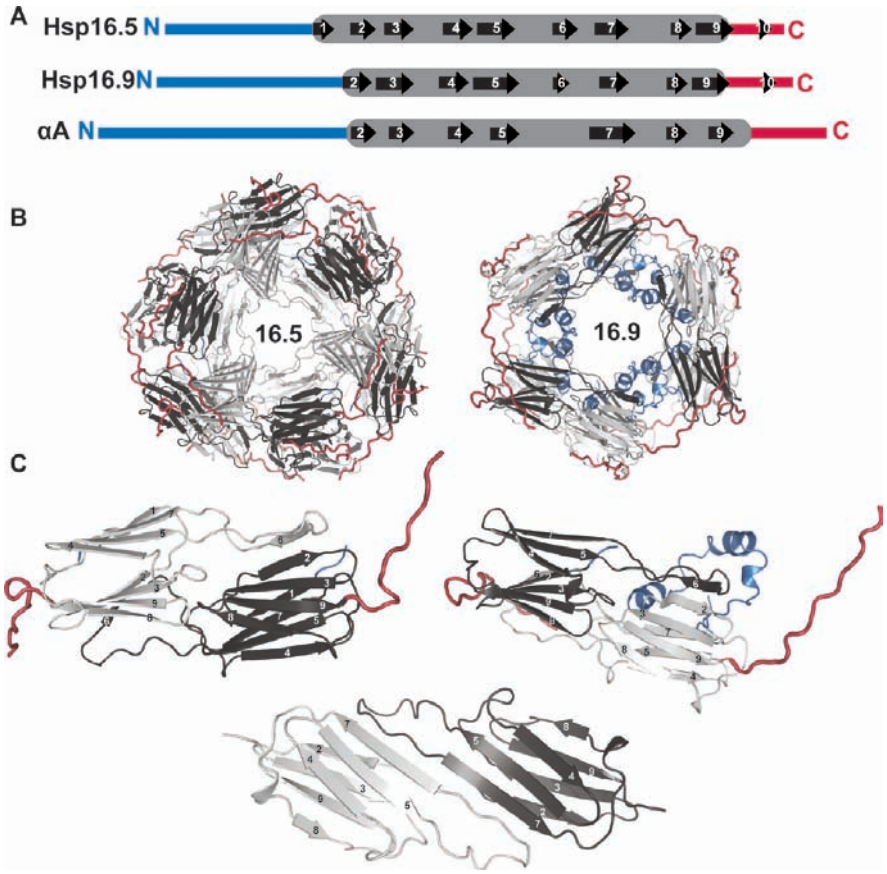

Figure 2: (a) comparison of the localization of the conserved α-crystallin domain in three sHsps. β-strands are marked as black arrows. (b) assembly of dimers of Hsp16.5 and Hsp16.9 into oligomers. (c) dimers of the sHsps in (a). Domain coloration is the same for all pictures. [5]

Oligomer formation under physiological conditions is another feature of sHsps. The αB-crystallin complex from *Homo sapiens* is shown in Figure 3, along with other sHsps for comparison. Whereas in most cases hollow spherical structures were found, Hsp16.9 from wheat exhibits a barrel-shaped structure, and αB-crystallin was found to be very polydisperse with a 24-mer as prevailing species. The newest reconstruction from cryo-electron microscopy (cryo-EM) renders another hollow spherical complex [7]. Figure 4 shows electron density representations of αB-crystallin viewed along the 2-fold symmetry axis and along two individual 3-fold symmetry axes (from left to right).

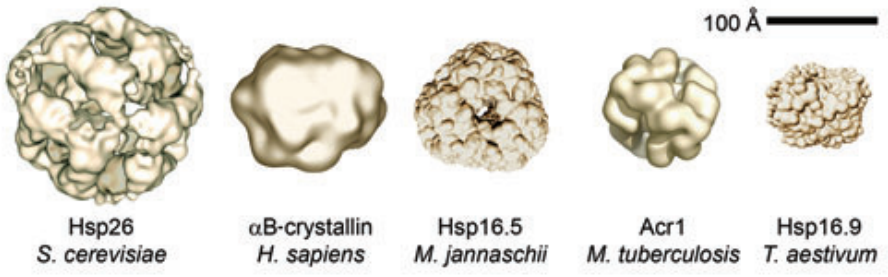

Figure 3: Quaternary structures of five sHsps. Cryo-EM reconstructions are displayed, except for M. jannaschii and T. aestivum where a crystal structure exists. Results of several authors are displayed as declared in Ref. [6].

Acquisition of crystal structures of un-modified wild-type sHsps is limited by the dynamic nature of the sHsps oligomer under investigation. αB complexes, for example, undergo continuous subunit exchange. This leads to a broad distribution of species that exist simultaneously, on the one hand, and to variable prevailing species under varied conditions, on the other hand. Moreover, subunit exchange takes place not only between complexes of the same protein, but also between complexes built from similar building blocks. Such *hetero-oligomers* were described for the combination of αA- and αB-crystallin, as well as αA-crystallin and Hsp27 [42]. *In vivo*, this exchange activity may lead to a large variety of sHsp complexes with distinct binding affinities - each adapted to individual substrates. It was further proposed that, by exposing otherwise buried hydrophobic patches, such subunit exchange constitutes a mechanism to discern unfolding intermediates in the cell [43][44]. Nevertheless, other results demonstrate that subunit exchange is not critical for sHsp chaperone activity including that of α-crystallins [45][46].

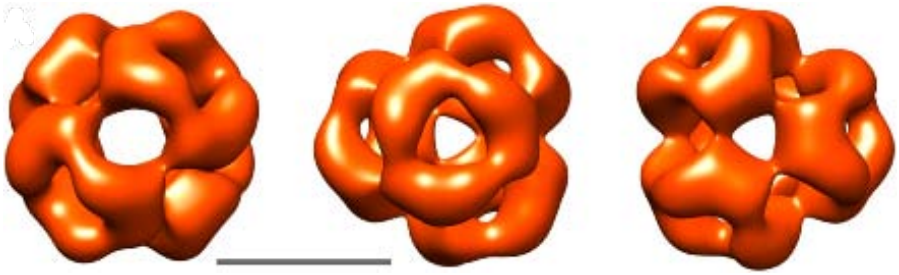

Figure 4: Electron density reconstruction of human αB-crystallin as obtained by EM viewed from three different perspectives. Scale bar: 10 nm [7]

Post-translational modification is an important issue in context with α-crystallins. Along with deamidation, oxidation, glycation and C-terminal truncation [47][25], stress induced phosphorylation of αB-crystallin is the primarily observed modification in *in vivo* studies. The predominant phosphorylation sites are serines at postion 19, 45 and 59. Involved kinases comprise p38 mitogen-activated protein (MAP) kinase and p44 MAP kinase [48]. Since the discovery of these phosphorylation sites, extensive studies on the relation between phosphorylation and chaperone activity were conducted [37][49][50][51]. Most of these studies were conducted with phosphorylation-mimicking mutations, i.e. serin to aspartate or glutamate conversions, which show interchangeable behavior with respect to oligomeric distribution [50], sub-cellular localization [52], and cellular trafficking [53]. Up to now, this has led to controverse communitations where some authors claim a decline of αB's chaperone capacity due to phosphorylation [50], whereas others describe a substantial amplification [37][5]. Increased subunit exchange was again discussed as an explanation for substrate binding amplification [37]. Once again, it seems that αB behaves differently depending on the target protein and the precise experimental specifications.

Finally, the interest in αB phosphorylation is further stimulated by its association with so-called protein misfolding diseases including aforementioned cataract (based on aggregated crystallin proteins), Alzheimer's (fibrillar β-amyloid plaques), Parkinson's (α-synuclein), Creutzfeldt-Jakob (prions), Huntington's (huntingtin) and Alexander's disease (glial fibrillary acidic protein) [25][54]. Except for cataract, these diseases include fibrillar plaques assembled from the stated proteins. However, sHsps - in particular αB - were detected in such plaques, too. Consequently, this rises the question about the involvement of αB in the pathological cause of the forenamed diseases. There is, at least, evidence implying a pathological attribute of αB phosphorylation [54][25]. A phosphorylation induced state with a constant high substrate affinity was discussed in this context [5].

1.2 THE HSP70 - HSP40 SYSTEM

Hsp70 plays a central role in the chaperone network of many cellular compartments of eukaryotes, eubacteria and many archaea. It consists of a N-terminal ATPase domain and a smaller C-terminal *lid* domain capable of binding elongated, unfolded stretches, only. Both domains interact mechanically with each other: binding of ATP leads to rapid peptide binding and release, with low affinity. Whereas ATP hydrolysis stimulates a high-affinity state with lower rates of binding and release. Nevertheless, the binding kinetics of Hsp70 are too slow to cope with aggregation, in the ATP *or* ADP bound state. This is where Hsp70's partner proteins come into play [17].

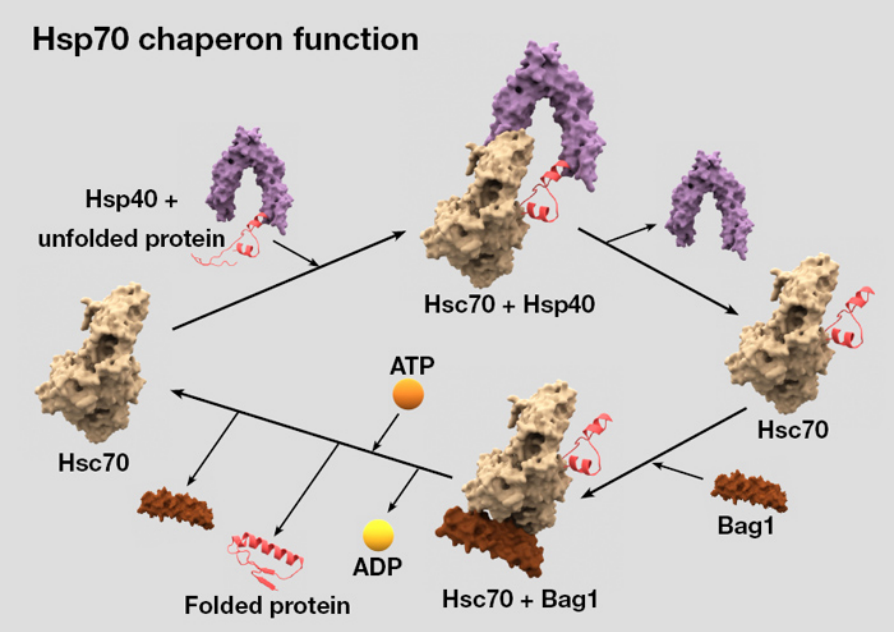

Figure 5: Chaperone mechanism of human Hsc70, Hsp40 and Bag1 [8][9]

The chaperone cycle of *human* cytosolic Hsp70, i.e. *70 kDa heat-shock cognate protein* (Hsc70), is illustrated by Figure 5. Hsp40 (top left) is in charge of initial substrate binding. In addition to the peptide binding domain, proteins of the Hsp40 class, including human Hdj1, share a conserved section of ca. 75 amino-acids which was named *J*-domain after *E.coli's* Hsp40 representative: DnaJ. The J-domain of Hsp40 is capable of association with Hsc70 ATPase domain in a way that promotes substrate transfer to Hsc70 (top). Additionally, Hsp40 promotes ATP hydrolysis which turns Hsc70 into its high-affinity mode (not depicted). After dissociation of the Hsp70/Hsp40 complex, Bag1 is bound to Hsc70 which mediates nucleotide exchange (bottom). By that, Hsc70 regains the low-affinity state and complete dissociation takes place. Although induction of conformational changes in the substrates have not been identified, substrate refolding upon cooperation of the Hsp70 system and small heat-shock proteins was demonstrated [30]. In this respect, the ensemble of Hsp70, J-domain co-chaperone and nucleotide-exchange factor is regarded as the simplest studied refolding system. Nonetheless, better yields are obtained by combining the Hsp70 system with a chaperonin [55][18].

1.3 OBJECTIVES

The aim of this thesis was, on the one hand, to gain a more distinct insight into the substrate interaction of αB-crystallin and the resulting substrate complexes (i), and on the other hand, to investigate the effects of αB phosphorylation on chaperone activity, along with the differences in substrate binding between phosphorylated and unphosphorylated αB (ii).

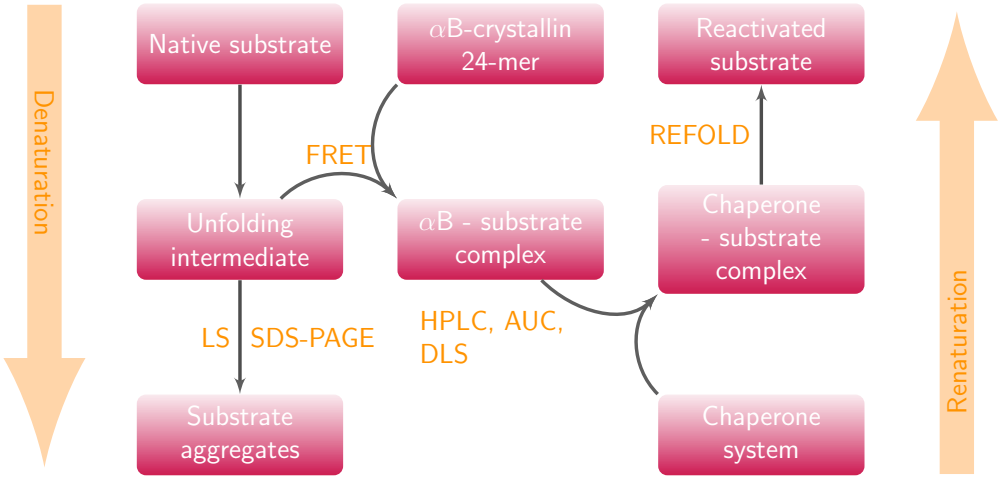

Figure 6: Outline of the processes investigated herein. The employed analyzation techniques are specified.

Figure 6 shows a flow chart of the studied processes within the αB - substrate system: a substrate is subjected to denaturation. At the stage of the unfolding intermediate, αB-crystallin binds the substrate by hydrophobic interactions, thus keeping it soluble during the stress situation. A chaperone system, namely Hsc70 and Hdj1, are subsequently employed to refold the substrate into its native assembly.

Formerly, much of the acquired knowledge about these processes was based on very *indirect* approaches, such as aggregation detection by light scattering (LS) or refolding monitored by changes in intrinsic fluorescence of the substrate. But, neither does LS say anything about the interaction taking place between αB and the substrate, nor does intrinsic fluorescence necessarily reveal *functional* recovery. Contrary to this, more profound methods shall be applied here.

The following key questions were devised:

- What is the rate of substrate binding? And how is it related to the rate of aggregation?
- What is the manifestation of the actually binding αB structure and the substrate - αB - complex?
- Is the Hsc70/Hdj1 system sufficient for substrate refolding? At which rates and yields?
- Does phosphorylation lead to an altered oligomerization state of αB?
- What is the effect of phosphorylation on the binding process and the substrate complexes?
- How does phosphorylation affect refolding?

In order to address these key issues, αB is being expressed and purified. Phosphorylation of αB is mimicked by replacing three distinct serine residues by glutamates. A FRET system shall be established to trace the substrate binding reaction. LS data about aggregation sup-

pression shall be confirmed by SDS-PAGE. High performance liquid chromatography (HPLC), analytical ultra-centrifugation (AUC) and dynamic light scattering (DLS) shall be applied to characterize the oligomeric species of αB (in the unmodified *and* phosphorylated state), as well as the respective substrate complexes. Finally, the Hsc70/Hdj1 system shall be optimized to refold αB bound substrate. The substrate recovery shall be tracked by means of a substrate activity assay.

2

MATERIALS

2.1 STRAINS & VECTORS

E.coli Mach1
Supplied by Invitrogen (Karlsruhe, Germany)
Genotype: F^{-} ϕ80(lacZ)ΔM15 ΔlacX74 hsd R($r_K^- m_K^+$)ΔrecA1398 endA1 tonA

E.coli BL21 (DE3)
Supplied by Stratagen (La Jolla, USA)
Genotype: F^{-} ompT gal dcm lon $hsdS_B$ (r_B^- m_B^-)λ(DE3 [lacI lacUV5-T7 gene 1 ind1 sam7 nin5])

Vector pET-28b(+)
supplied by Merck (Darmstadt, Germany)

2.2 PROTEINS

Name:	*Source:*
αA-Crystallin	kindly provided by J. Peschek
αB-Crystallin, wt	purification described herein
αB-Crystallin, mut.	purification described herein
Human DnaJ homologue (Hdj1)	purification described herein
Heat-shock cognate protein (Hsc70)	kindly provided by J. Peschek
L-Lactate dehydrogenase (LDH)	Roche (Mannheim, Germany)
Luciferase	Roche (Mannheim, Germany)
Lysozyme	Sigma-Aldrich (Saint Louis, USA)
Malate dehydrogenase (MDH)	Roche (Mannheim, Germany)
Pyruvate kinase (PK)	Roche (Mannheim, Germany)

2.3 CHEMICALS

Chemical Substance:	*Manufacturer:*
Acrylamide (38%, 2% Bisacrylamide)	Roth (Karlsruhe, Germany)
Adenosin-5´-triphosphate (ATP), Disodiumsalt	Roche (Mannheim, Germany)
Agarose, research grade	Serva (Heidelberg, Germany)
Ammoniumperoxodisulfate (APS)	Roche (Mannheim, Germany)
Ammonium sulfate	Merck (Darmstadt, Germany)
Atto550 maleimide	Atto-Tec (Siegen, Germany)
Bacto Agar	Difco (Detroit, USA)
Bacto Tryptone	Difco (Detroit, USA)
Bacto Yeast Extract	Difco (Detroit, USA)
Bromphenolblue S	Serva (Heidelberg, Germany)
Calcium chloride	Merck (Darmstadt, Germany)
Complete Protease Inhibitor Mix G	Roche (Mannheim, Germany)
Coomassie Brilliant-Blue R-250	Serva (Heidelberg, Germany)
Coomassie Protein Assay Reagent	Pierce (Rockford, USA)
Dimethyl sulfoxide (DMSO)	Roth (Karlsruhe, Germany)
dipotassium hydrogenphosphate	Merck (Darmstadt, Germany)
Disodium hydrogen phosphate	Roth (Karlsruhe, Germany)
5,5'-Dithio-bis-Nitrobenzoic acid (DTNB)	Sigma (St. Louis, USA)
1,4-Dithiothreitol (DTT)	Roth (Karlsruhe, Germany)
Ethylendiamintetraacidic acid (EDTA)	Merck (Darmstadt, Germany)
Ethanol, p.a.	Riedel de Haen AG (Seelze, Germany)
Ethidium bromide	Roth (Karlsruhe, Germany)
Formaldehyde, 37% p.A.	Roth (Karlsruhe, Germany)
Glutathione, reduced form (GSH)	Roche (Mannheim, Germany)
Glycerol, 99%	ICN (Costa Mesa, USA)
Glycine	Roth (Karlsruhe, Germany)
Hydrochloric acid	Roth (Karlsruhe, Germany)
4-(2-hydroxyethyl)-1-piperazineethanesulfonic acid (HEPES)	Roth (Karlsruhe, Germany)
Isopropanol	Roth (Karlsruhe, Germany)
Isopropyl-β-D-thiogalaktopyranosid (IPTG)	Roth (Karlsruhe, Germany)

β-Mercaptoethanol, pure	Merck (Darmstadt, Germany)
Magnesium chloride	Merck (Darmstadt, Germany)
Magnesium sulfate	Merck (Darmstadt, Germany)
Nicotinamide adenine dinucleotide, sodium salt(NADH)	Roch (Mannheim, Germany)
N,N,N´,N´-Tetramethylethylendiamin (TEMED)	Roth (Karlsruhe, Germany)
Oxaloacetat	Sigma-Aldrich (Steinheim, Germany)
Phosphoenolpyruvic acid (PEP)	Roche (Mannheim, Germany)
Phosphoric acid	Roth (Karlsruhe, Germany)
Potassium chloride	Roth (Karlsruhe, Germany)
Potassium dihydrogenphosphate	Merck (Darmstadt, Germany)
Sodium carbonate	Roth (Karlsruhe, Germany)
Sodium chloride	Roth (Karlsruhe, Germany)
Sodium dodecylsulfat (SDS)	Roth (Karlsruhe, Germany)
Sodium hydroxide	Roth (Karlsruhe, Germany)
Tris-(Hydroxymethyl)-aminomethan (Tris)	Roth (Karlsruhe, Germany)

2.4 UTENSILS FOR MOLECULAR BIOLOGY & EXPRESSION

Product:	*Manufacturer:*
Ampicillin	Roth (Karlsruhe, Germany)
BSA	Promega (Mannheim, Germany)
dNTP	Roth (Karlsruhe, Germany)
Kanamycin	Roth (Karlsruhe, Germany)
LB-Broth (Lennox)	Roth (Karlsruhe, Germany)
Div. primers	MWG-biotech AG (Ebersberg, Germany)
PCR 10x buffer for Pwo + $MgCl_2$	Roche (Mannheim, Germany)
Pwo polymerase	Roche (Mannheim, Germany)
Restriction enzymes (Nco, NotI)	Promega (Mannheim, Germany)
Restrictive digestion buffer D	Promega (Mannheim, Germany)
T4-Ligase	Roche (Mannheim, Germany)
Wizard MiniPrep Kit	Qiagen GmbH (Hilden, Germany)
Wizard PCR Purification Kit	Qiagen GmbH (Hilden, Germany)
Thermo cycler primus 25	Peqlab (Erlangen, Germany)

Solutions:	*Component:*	*Quota:*	
TB solution	HEPES	10	mM
	$CaCl_2$	15	mM
	KCl	250	mM
	H_2O		
	KOH / HCl	adjust pH to 6.7	
	$MnCl_2$	55	mM
1000 x Ampicillin stock	Ampicillin	10	mg/ml
1000 x Kanamycin stock	Kanamycin	35	mg/ml

2.5 PURIFICATION EQUIPEMENT

Columns

Q Sepharose (150 ml)	GE Healthcare (Piscataway, USA)
Superdex 200 Prep Grade (250 ml)	GE Healthcare (Piscataway, USA)
Resource-Q, Source 15 (6 ml)	GE Healthcare (Piscataway, USA)
SP Sepharose fast flow	GE Healthcare (Piscataway, USA)

Buffers for α purification

TE lysis buffer pH 10	Tris	50	mM
	EDTA	2	mM
NTE elution buffer pH 10	NaCl	1	M
	Tris	50	mM
	EDTA	2	mM
TNE gel filtration buffer pH 10	Tris	50	mM
	NaCl	50	mM
	EDTA	2	mM

Buffers for Hdj1 purification

HE lysis buffer pH 7	HEPES/NaOH	25	mM
	EDTA	1	mM
	DTT	2	mM
NHE elution buffer pH 7	NaCl	1	M
	HEPES/NaOH	25	mM
	EDTA	1	mM
	DTT	2	mM

Dialysis buffer

Phosphate Buffer	NaCl	150	mM
	$Na_2HPO_4 \cdot 2H_2O$	10	mM
	KH_2PO_4	2.5	mM

Centrifuges

Rotina 46 R Centrifuge	Hettich (Tuttlingen, Germany)
Eppendorf-Centrifuge 5415 C	Eppendorf (Hamburg, Germany)
Avanti J25	Beckman Coulter (Fullerton, USA)
Rotor JA-10 and JA-25.50	Beckman Coulter (Fullerton, USA)

Cell Disruptor

Basic Z	Constant Systems (Warwick, UK)

Purification system

ÄKTA FPLC	GE Healthcare (Piscataway, USA)
Frac-900 fraction collector	GE Healthcare (Piscataway, USA)
Superloops 150 / 50 ml	GE Healthcare (Piscataway, USA)
Additional Tools	
Ultra filtration cell 8050	Amicon (Danvers, USA)
Amicon-Ultrafiltration Membrane YM10/30/100	Millipore (Bedford, USA)
Centricon 10/30/100-microconcentrators	Millipore (Bedford, USA)
Dialysis tubes Spectra/Por (6-8 kDa)	Spectrum (Houston, USA)

2.6 analytical instruments & components

Agarose Gel Electrophoresis:

Electrophoresis device RHU10X	Roth (Karlsruhe, Germany)
UV-scanner Image Quant 300	GE Healthcare (Piscataway, USA)
1 kb DNA Ladder Molecular Weight Standard	New England Biolabs (Beverly, USA)

BJ Buffer for DNA Analysis	Glycerol	50	% (v/v)
	EDTA (pH 8.0)	10	mM
	Bromphenolblue	0.2	% (w/v)
	Xylencyanol	0.2	% (w/v)
1% Agarose-Solution	Agarose	1	g
	TAE (1x)	100	ml
	Ethidiumbromide solution	10	µl
TAE (50x) pH 8.0	Tris acetate pH 8.0	2	M
	EDTA	50	mM

Analytical Ultra-Centrifugation:

Centrifuge XL-A	Beckman Coulter (Fullerton, USA)
An-60 Ti Rotor (4-Place)	Beckman Coulter (Fullerton, USA)

Circular Dichroism Spectropolarimetry:

CD Spectropolarimeter Jasco J715	Jasco (Groß-Umstadt, Germany)
Peltier temperature device PTC 343	Jasco (Groß-Umstadt, Germany)
CD-Cuvette 0.35 ml	Hellma (Müllheim, Germany)

Fluorescence Spectroscopy:

Spectrofluorometer FluoroMax-3	HORIBA Jobin Yvon (Edison, USA)
Spectrofluorometer FluoroMax-4	HORIBA Jobin Yvon (Edison, USA)
Temperature adjustable cuvette retainer	HORIBA Jobin Yvon (Edison, USA)
Fluorescence cuvette 1.5 ml	Hellma (Müllheim, Germany)
Lucifer yellow iodoacetamide (LYI)	Invitrogen (Carlsbad, USA)

Atto550 maleimide	Atto-Tec (Siegen, Germany)
Succinimidyl ester5(6)-TAMRA	Invitrogen (Carlsbad, USA)

High Performance Liquid Chromatography:

HPLC-Instrument	Jasco (Großumstadt, Germany)
Pump system: PU-1580	Jasco (Großumstadt, Germany)
Fluorescence detector: FP-920	Jasco (Großumstadt, Germany)
UV-detector: UV-1575	Jasco (Großumstadt, Germany)
TSK G4000PW HPLC Gel Filtration Column	Tosoh Bioscience (Stuttgart, Germany)
Kit for molec. weights 29 - 700 kDa	GE Healthcare (Piscataway, USA)

Balances:

BP 1500 S	Satorius (Göttingen, Germany)
AC 2115	Satorius (Göttingen, Germany)

SDS-PAGE:

Hoefer Mighty Small II	Amersham Bioscience (Freiburg, Germany)
Low-Range Molecular Weight Standard	BioRad Laboratories (Munich, Germany)
ImageScanner III	GE Healthcare (Piscataway, USA)

Separation gel 15 %	Acrylamide 40 %	3.75	ml
	water	3.75	ml
	4 x SDS buffer	2.5	ml
	(0.8% SDS, 1.5 M Tris/HCl, pH 8.8)		
Stacking gel	Acrylamide 40 %	0.625	ml
	water	1.875	ml
	2 x SDS buffer	2.5	ml
	(0.4% SDS, 0.25 M Tris/HCl, pH 8.8)		
SDS-Running Buffer (10x)	Tris	0.25	M
	Glycine	2	M
	SDS	1	% (w/v)
Laemmli Sample Buffer (5x)	SDS	10	% (w/v)
	Glycerol	50	% (w/v)
	Tris	300	mM
	Bromphenolblue	0.05	% (w/v)
	β-Mercaptoethanol	5	% (w/v)
Fairbanks Solution A	Isopropanol	25	% (v/v)
	acetic acid (technical grade)	10	% (v/v)

	Coomassie blue R	0.05	%
Fairbanks Solution D	acetic acid (technical grade)	10	% (v/v)

UV-Vis Spectroscopy:

Varian Cary 50 Bio UV-Vis-Spectrophotometer	Varian (Palo Alto, USA)
Novaspec II	Pharmacia (Uppsala, Sweden)
Nanodrop ND 1000	Peqlab (Erlangen, Germany)
UV-cuvettes 0.1 ml	Hellma (Müllheim, Germany)
Polystyrol cuvettes 1.5 ml	Sarstedt (Nümbrecht, Germany)

2.7 SOFWARE

Software:	*Developer:*
Bibdesk	Michael O. McCracken *et al.* (bibdesk.sourceforge.net/)
BioEdit	Tom Hall (North Carolina State University, USA)
Geneious	Biomatters Ltd (Auckland, New Zealand)
Gnuplot 4.3	Thomas Williams *et al.* (sourceforge.net/projects/gnuplot)
ProtParam	Swiss Institute of Bioinformatics (Lausanne, Switzerland)
Sedfit	Peter Schuck (Bethesda, USA)
TeX Live 2009	TUG (Portland, USA)
TexShop 2.33	Richard Koch *et al.* (Eugene, USA)

2.8 FURTHER EQUIPEMENT

Product:	*Manufacturer:*
Cellulose Acetate Filter 0.45µm	Santorius (Goettingen, Germany)
Div. cups	Eppendorf (Hamburg, Germany)
Digital Heatblock	VWR (Darmstadt, Germany)
Eppendorf-Thermomixer	Eppendorf (Hamburg, Germany)
Freezer	Liebherr (Lienz, Austria)
Div. glassware	Schott Duran (Wertheim/Main, Germany)
Gloves	Meditrade (Kiefersfelden, Germany)
Ice Maker	Ziegra (Isernhagen, Germany)
Incubator	New Brunswick Scientific (Nürtingen, Germany)
Magnet Stirrer Heidolph MR2000	Heidolph (Kehlheim, Germany)
Membrane Filter 0.2µm	Whatman (Dassel, Germany)
Membrane Vacuum Pump	Vacuubrand GmbH (Wertheim, Germany)
Metal Thermostat TB 1	Biometra (Göttingen, Germany)
Nitrogen, liquid	Linde AG (Munich, Germany)
Parafilm	Pechiney (Menasha, USA)
pH-Meter	WTW (Weilheim, Germany)
pH-Indicator paper	Roth (Karlsruhe, Germany)
Div. Pipettes Pipetman	Gilson (Middleton, USA)
Sterile Filter, syringe driven	Millipore (Cork, Ireland)
Sterile Syringes	Terumo (Leuven, Belgium)
Sterile Needles	Braun (Melsungen, Germany)
Tips for pipettes	Sarstedt (Sarstedt, Germany)
Div. tubes	Greiner Bio-One (Kremsmünster, Austria)
Ultra Low Temperature Freezer	New Brunswick Scientific (Edison, USA)
Varioklav	EPZ H+P (Oberschleißheim, Germany)
Voltage Source GPS 200/400	Pharmacia (Uppsala, Sweden)
Water bath	Haake F6-K (Karlsruhe, Germany)

3

METHODS

3.1 PREPARATIVE METHODS

3.1.1 *Molecular Biology Methods*

Within the scope of this thesis eight mutants were cloned on the basis of the *CRYAB* gene, which encodes for human wild type αB-crystallin. Primers used herein were designed by J. Peschek using the BioEdit software for specific gene amplification and purchased from *MWG-biotech AG*. A table of all the used primers can be found in the appendix A.1.

Mutagenesis

Three different phospho-mimetic serin to glutamate mutations were introduced at positions 19, 45 and 59 of the wild type amino acid sequence. To this end, linker PCR (polymer chain reaction) was employed.

In the first reaction of this approach only half-constructs are amplified as illustrated in Figure 7. They reach either from the beginning of the template gene (5'-end) to the desired mutation, or from this mutation to the end of the gene (3'-end).

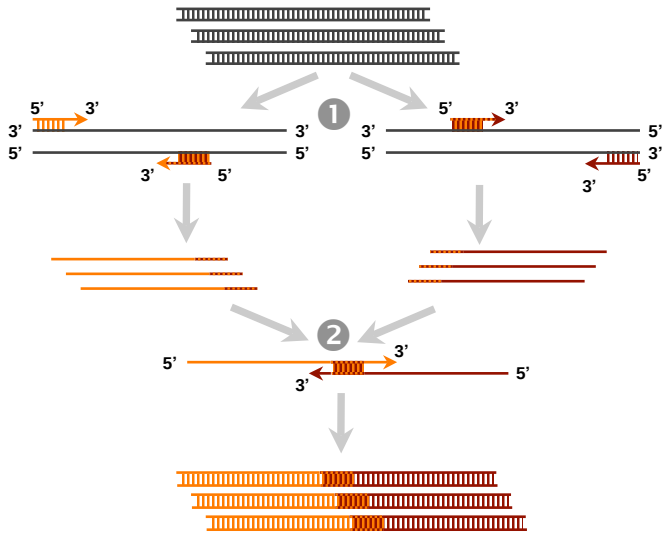

Figure 7: Schematic illustration of the Linker PCR approach (not to scale). A first reaction generates the half-constructs (1). Around the inserted mutation, they share a short DNA section. In a second reaction, this segment primes the fusion of both halves to give the full-length mutant gene.

Only in a second step, linkage of both half-constructs gives the complete mutated sequence. For this purpose, the template sequence in the general ansatz (Table 15) is substituted by equal amounts of the corresponding half-constructs. Specific hybridization and good yields were achieved by applying an annealing temperature of 65°C.

Each polymerase chain reaction was followed by evaluation via agarose gel electrophoresis (see Section 3.2.1). PCR products were excised from the gel if required by diffuse bands. The concentration of the PCR-products was determined using the *Nanodrop* spectrometer in order to estimate the quantities for following reactions.

Prior to further operations, the product was purified with the *PCR clean up kit* according to the protocol of the manufacturer.

For further cloning of double or triple mutants, this procedure was repeated based on a single-mutant template.

Table 15: General PCR specifications.

Ansatz:		*Thermo-cycling protocol:*		
5 µl	10x PCR buffer for Pwo + Mg^{2+}	2 min	94°C	
5 µl	dNTP (10 mM each)	0.5 min	94°C	35 loops
0.5 µl	αB_{WT}-pET28b(+)	1 min	65°C	
0.5 µl	For. primer	1 min	72°C	
0.5 µl	Rev. primer	5 min	72°C	
0.5 µl	Pwo-polymerase			
38 µl	Nuclease-free water			

Additionally a cysteine was introduced into the above triple mutant. Since αB_{WT} includes no cysteins, this was required for site-directed fluorescent thiol-labeling. The cysteine was inserted at position four (A4C) in a one-step reaction applying the general settings of Table 15

The Vector & insertion of the target gene

A pET-28b(+) vector was chosen as a carrier for the transfer of the gene product into the cell (see Figure 8). It comprises many restriction sites; among those Nco I and Not I, which were used herein.

The restrictive digest of the vector, as well as the insert, was carried out according to Table 16 during 3 hours of incubation at 37°C. The product was subsequently evaluated by agarose gel electrophoresis and purified.

To avoid religation of the cut vector, its ends were dephosphorylated by incubating the mixture in Table 17 for 2 hours at 37°C. Finally, ligation of the gene into the vector was performed with the ansatz in Table 18 for 12 min at room temperature.

Table 16: Ansatz for the restrictive digest.

25 µl	PCR product or vector
0.5 µl	Nco I
0.5 µl	Not I
0.3 µl	BSA
3 µl	10x buffer D

Table 17: Ansatz for dephosphorylation.

88 µl	cut vector
10 µl	10x reaction buffer
2 µl	alkaline phosphatase

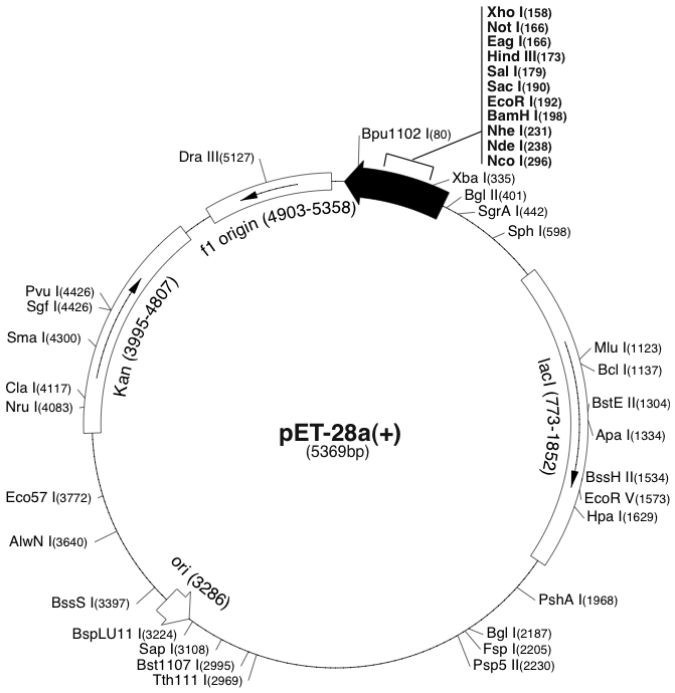

Figure 8: Vector map of pET-28c(+) which differs from the utilized pET-28b(+) by one base pair only (*Novagen/Merck, Darmstadt, Germany*).

Table 18: Ligation ansatz.

10 µl	Quick Ligation buffer
5 µl	nuclease-free water
4 µl	cut insert
1 µl	cut, dephosph. vector
1 µl	T4 ligase

Preparation of ultra-competent cells

Starting with an over-night culture of Mach1 cells on a Luria broth (LB) agar plate, about ten colonies were picked under sterile conditions and employed to inoculate 250 ml of LB media containing 10 mM $MgCl_2$ and 10 mM $MgSO_4$ in a 1 l flask. The culture was incubated over-night at 20°C while shaking. Once an optical density (OD_{600}) of 0.5 at 600 nm was reached, the culture was cooled down on ice for 10 min and pelleted at 4000 rpm and 4°C for 10 min. The cells were gently resuspended with 80 ml of ice-cold TB solution and kept on ice for 10 min. Pelleting and resuspending were repeated with 20 ml ice-cold TB solution including 1.4 ml DMSO. After this procedure, the cells are receptive to transformation. They were aliquoted and stored at -80°C if not immediately transformed. (Adapted from Inoue *et al.* [56])

Transformation

50 µl of Mach1 ultra-competent cells, together with 10 µl of ligated plasmid were incubated on ice for 20 min. The cells underwent a 1 min heat-step at 42°C and were cooled down on ice again. 1 ml of LB media was added, and everything incubated at 37°C for 40 min before the cells were plated on LB agar plates containing 35 µg/ml kanamycin (LB_{kana}). The cells were grown at 37°C over-night [57].

At this point, 3 ml LB tubes were inoculated by single colonies picked from the plates. After 6 hours of incubation at 37°C while shaking, the dense cultures were purified with the *MiniPrep Kit* and sent for sequencing to *GATC Biotech AG* (Konstanz, Germany).

Once checked for the desired gene, the cells were transformed into the expression strain, BL21, applying the aforementioned procedure.

3.1.2 *Protein expression & purification*

All the culture broths used herein were autoclaved, and all the purification buffers filtrated and degased.

Expression & Harvesting

For the expression of the target gene, a 100 ml culture of transformed BL21 cells was grown in LB_{kana} (LB_{amp} in the case of Hdj1 expression) over-night at 37°C while shaking. Three 2.5 l expression flasks with the same media were inoculated by 20 ml over-night culture each, and cultivated at 37°C. At OD_{600} = 0.6 - 0.8, the expression was induced by 1 mM isopropyl β-D-1-thiogalactopyranoside (IPTG).

After 12 hours of expression at 30°C, the cells were harvested by centrifugation (12 min, 7.5 krpm, 6°C). The pellet was then resuspended in max. 150 ml TE lysis buffer (HE lysis buffer for Hdj1 purification) plus added protease inhibitor mix G. Cell lysis was accomplished at 2 kbar by a cell disruptor. The lysate was subsequently centrifuged for 20 min at 20 krpm and 6°C and the supernatant was collected in a pre-cooled flask.

Purification of αB-crystallin

Succeeding cell harvesting, the yield was subjected to three preparative chromatography steps using an *ÄKTA FPLC* system.

To begin with, anion exchange chromatography (AEC) was performed using a self-packed Q-Sepharose column equilibrated in TE buffer. Elution of the protein was attained under a linear salt gradient between TE and NTE buffer (1 M NaCl). Fractions were collected (8 ml), analyzed by SDS-PAGE and accordingly pooled.

The resulting product was reconcentrated to a volume of 45 ml using an amicon cell and a 30 kDa millipore membrane. A Superdex200 gel filtration column equilibrated in TNE buffer (100 mM NaCl) was loaded with the protein by means of a 50 ml superloop in three runs. Analysis of the collected 3 ml fractions by SDS-PAGE led to a new accumulation.

The product was dialyzed over-night in low-salt TE buffer, before a second AEC step was performed, using a ResourceQ column. The buffers and the linear salt concentration gradient were identical to the first AEC step. Once more, the 2.5 ml fractions were pooled according to the result of SDS gel electrophoresis. The pool was dialyzed against phosphate buffer (PBS) and again reconcentrated with the amicon cell. Aliquotes of 200 µl were shock-frozen in liquid nitrogen and stored at -80°C.

The two αB-crystallin mutants, αB-3E and αB-A4C-3E, were purified according to the same procedure. Except for an additional ammonium sulfate-precipitation step prior to gel filtration of the latter mutant. To this end, the salt concentration of the purification product was gradually increased to 30 % of the NH_4SO_4-saturation concentration. After incubation at 4°C for 45

min, the solution was centrifuged at 15 krpm for 15 min. In a second gradient the NH_4SO_4 concentration of the decanted supernatant was increased to 75 %. After centrifugation with equal settings, the pellet was resuspended with TNE buffer and loaded onto the Superdex200 column.

Purification of the human DnaJ homologue (Hdj1)

Following cell harvesting, the cleared lysate was first loaded onto a pre-equilibrated SP-Sepharose column. The protein elution was achieved by applying a linear gradient from low-salt HE lysis buffer to high-salt NHE elution buffer. 6 ml fractions were collected, analyzed by SDS-PAGE, pooled correspondingly and reconcentrated to 30 ml employing the amicon cell.

This volume was subjected to gel filtration chromatography: a Superdex200 column was used with PBS as running buffer. Fractions of 3 ml were collected and validated by SDS-PAGE. This revealed pure protein fractions, which were reconcentrated, aliquoted, and shock-frozen in liquid nitrogen before storage at -80°C.

3.2 ANALYTICAL TECHNIQUES

3.2.1 *Gel electrophoresis*

Agarose Gel

1% Agarose-Solution (see Section 2) containing 0.4 µg/ml ethidium bromide was poured into the respective mold. When set, the gel was loaded with a 1 kb molecular weight standard, along with the samples, and run in TAE running buffer employing the *RHU10X* electrophoresis device.

Finally, the gels were captured using the UV-scanner, Image Quant 300.

SDS-Polyacrylamide gel-electrophoresis

Gels consisting of a 15 % separating gel and a stacking gel were cast employing the Hoefer Mighty Small II apparatus (gel dimensions: 7 x 9 x 0.075 cm^3). A dentate mold was applied for easier sample administration. Cross-linking of the gels was initiated by 0.1 (v/v) % TEMED using 0.1% (v/v) ammonium peroxodisulfate as a radical carrier.

After mixing with Laemmli sample buffer, the samples were heated up to 95°C before measurement. Electrophoresis was performed vertically at 30 A per gel for 45 min. This SDS-PAGE method was adapted from Fling & Gregerson [58].

Staining of the gels was done after a protocol, modified from Fairbanks *et al.* [59]. Staining by Fairbanks solution A was directly followed by destaining using Fairbanks solution D. In both cases the solution was heated up in order to decrease incubation time.

Stained gels were scanned by the ImageScanner III.

3.2.2 *Spectrometry*

All measurements were carried out in PBS unless stated differently.

CD Spectroscopy

Circular dichroism (CD) was measured with a temperature-controlled *CD Spectropolarimeter, Jasco J715*, at 20°C in the respective dialysis buffer or in PBS. A 350 µl CD-cuvette with an optical path-length of 0.1 cm was utilized. Data was averaged over 20 consecutive runs, and corrected for the buffer spectrum.

Information about the secondary structure of 0.1 - 0.2 mg/ml protein samples was acquired by far-UV scans ranging from 195 - 260 nm.

This is the range where the amides of the protein backbone leave there CD-fingerprint: α-helices or β-sheets exhibit well defined torsional angles ϕ, ψ along the protein backbone. The resulting distinct orbital alignment leads to differential interaction with electromagnetic waves depending on their polarization [10]. The orientations of the transition dipoles and the electronic transitions are displaye in Figure 9 (a).

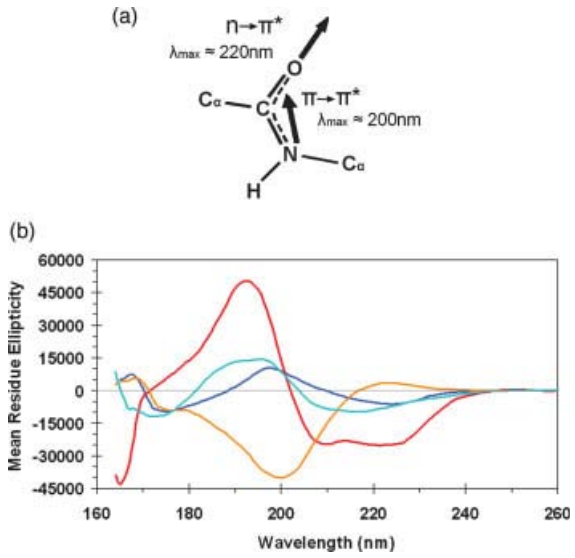

Figure 9: (a) A peptide bond with indicated orientation of the transition dipoles (thick arrows), corresponding electronic transitions and their energy range in nm. (b) Characteristic CD spectra: the α-helical protein myoglobin (red), concanavalin A (blue) and beta-lactoglobulin (cyan) both predominantly including β-sheets and collagen (orange) with poly-proline II helices. [10]

This difference between the absorbance of right and left polarized light is recorded in a CD spectrum. Therefore, it incorporates information about the content of secondary structure in the protein under investigation (cf. Figure 9 (b)): α-helices display a negative band near 222 nm and a length-dependent signal at 208 nm (negative) and 195 nm (positive). Whereas β-sheets are more difficult to reveal by a less intense negative band at 216 nm, and a positive one between 195 and 200 nm [60].

UV/VIS Spectroscopy

Spectra and kinetic measurements were performed on a temperature-controlled *Varian Cary 50 Bio* UV-Vis-Spectrophotometer employing non-absorbing quartz UV-cuvettes (optical path-length = 1 cm). A baseline correction was carried out for all measurements.

Concentrations were determined according to the Lambert-Beer law [61] shown in Equation 3.1: A_λ absorbance at wavelength λ, I, I_0 intensity of the transmitted and the incident light, respectively, ϵ_λ extinction coefficient of the dissolved species, d optical path-length, c concentration. The extinction coefficients of the proteins were obtained from *ProtParam* a front-end tool for parameter calculation from the *ExPASy Proteomics Server* [62].

$$A_\lambda = -\log_{10}\left(\frac{I}{I_0}\right) = \epsilon_\lambda \cdot d \cdot c \tag{3.1}$$

The same spectrometer was also applied to measure light scattering by protein aggregates. Data was acquired at a wavelength of 350 nm where protein samples do not absorb light. Hence, the loss of transmitted light was equal to the portion of scattered light.

Flourescence Spectroscopy

Fluorescence was measured with temperature-controlled *Spectrofluorometers* and stirred fluorescence cuvettes. A custom-built software extension allowed for acquisition of kinetics data at two wavelengths during the same experiment.

For fluorescence resonance energy transfer (FRET) measurements the respective proteins were labeled with either lucifer yellow iodoacetamide, *Atto550* maleimide or tetramethyl-rhodamine (TAMRA) succinimidyl ester according to the supplier's protocol. Labelling efficiencies were between 20 and 50 %.

The phenomenon underlying FRET is a non-radiative energy transfer, which takes place between two chromophores. If a dye molecule is excited by external electro-magnetic radiation, it can regain its ground state not only by emissive fluorescent or phosphorescent relaxation, but also by many other non-radiative processes (see Figure 10a) [63].

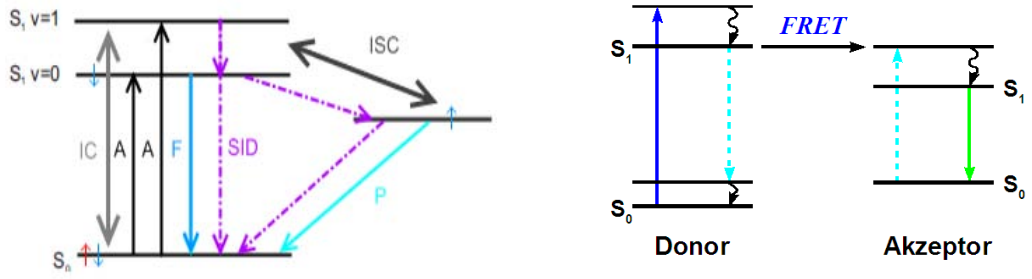

(a) (b)

Figure 10: Different relaxation pathways: (a) after excitation by absorption (A) of a photon, relaxation may occur by fluorescence (F), inter system crossing (ISC) followed by phosphorescence (P), internal conversion (IC) or radiation-less deactivation (SID) [11]. (b) Alternatively, non-radiative FRET can lead to excitation followed by fluorescence in a second species with suitable energy level spacing [12].

FRET represents an additional decay process (see Figure 10b), due to interactions of the transition dipole moments of a donor p_{ji} and an acceptor chromophore p_{kl}. A precondition is thereby the preferably large overlap integral between the donor's emission spectrum and the acceptor's absorption spectrum.

An efficient transfer requires further that donor and acceptor are in close proximity, because the transition dipole-dipole interaction - and hence the energy transfer rate $k_T(r)$ (Equation 3.2) - is proportional to r^{-6}.

$$k_T(r) = \frac{1}{\tau_D}\left(\frac{R_0}{r}\right)^6 \tag{3.2}$$

$${R_0}^6 \propto \kappa^2 = (\cos\theta_{DA} - 3\cos\theta_D \cos\theta_A)^2 \tag{3.3}$$

Equation 3.2 shows that the rate of transfer is proportional to the decay rate of the donor. The Förster radius R_0 is thereby defined as the distance at the efficiency half-maximum. It should ideally lie between 2 and 9 nm [64].

Finally, the Förster radius itself depends on the spatial orientation of the interacting dipoles by Equation 3.3 [65].

3.2.3 *Analytical Chromatography*

High performance liquid chromatography (HPLC) was measured at 20°C using a *TSK G4000PW* HPLC gel filtration column with filtrated and degased PBS as running buffer at a flow rate of 1 ml/min. Applying this settings, the pressure remained below 3 $kg \cdot cm^{-2}$. Data was acquired simultaneously from connected UV-absorption and fluorescence detectors.

The system was calibrated with molecular weight standards of 29 - 669 kDa, which produced a straight calibration line when plotted semi-logarithmically.

In order to avoid clogging of the column, the samples were either filtrated (calibration standards) or centrifuged (heat incubated samples) before 100 µl of each were injected.

3.2.4 *Analytical Ultra-Centrifugation*

A *Beckman XL-A* analytical ultra-centrifuge with an absorption detector was used for sedimentation velocity experiments conducted at 20°C and 30 krpm.

The samples were pre-incubated at 45°C for 45 min prior to the measurement. The samples exhibited an absorbance of 0.7 - 0.8 at a path-length of 1.2 cm. Data is corrected for the buffer background.

There are two principal modes of experiments using an analytical ultra-centrifuge (AUC). During *sedimentation equilibrium* runs, information about thermodynamic properties can be acquired. On the other hand, the *sedimentation velocity* experiments implemented herein, allow for hydrodynamic characterization (e.g.: particle size, shape etc.) of the species present in solution.

In contrast to HPLC, AUC requires no auxiliary matrix to dissect the species in a sample. The separating effect is exerted exclusively by the centrifugal force. This is a big advantage, since the protein remains in its original buffer environment. Thus, any artificial interactions are precluded.

During sedimentation velocity measurements the sedimentation process caused by centrifugation is traced. In our case, a UV absorption detector continually scanned the sector-shaped sample cell. By this, changes in the concentration distribution are recorded. Figure 11 gives an example of such data. Such changes result from sedimentation from the inner border to the outer bottom, but also from buoyancy, hydrodynamic friction and diffusion. Alternatively, fluorescence or interference detectors can be employed, too.

Sedimentation is described by the Svedberg Equation 3.4. The sedimentation coefficient s (in units of Svedbergs) depends on the radial velocity of the protein in the sample cell u, the angular velocity of the rotor ω, and the radius r. From this known data, along with the partial volume of the protein $\overline{v}$, the solvent density ρ and the molar mass M, the friction factor f is obtained from comparison with a compact sphere. Where the latter is accessible by Stokes' equation. [13]

$$s = \frac{u}{\omega^2 r} = \frac{M(1-\overline{v}\rho)}{N_A f} = \frac{MD(1-\overline{v}\rho)}{RT} \tag{3.4}$$

$$\frac{\partial \chi(r,t)}{\partial t} = \frac{1}{r}\frac{\partial}{\partial r}\left[rD\frac{\partial \chi(r,t)}{\partial r} - s\omega^2 r^2 \chi(r,t)\right] \tag{3.5}$$

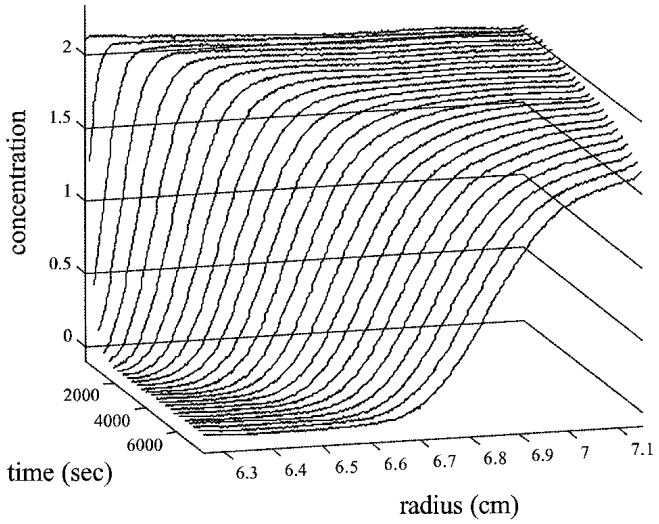

Figure 11: Exemplary data of a AUC measurement. [13]

Moreover, multi-meric assemblies are revealed by todays fitting programs. In contrast to the early days when the center point of the concentration boundary (i.e. the inflection point of the absorption curve) represented the entire data basis, modern computers make it possible to model the concentration distribution and its evolution by the Lamm Equation 3.5. Being the underlying transport equation, it extends the data basis to the full set of data points by relating the temporal alteration of the concentration distribution χ to its radial, diffusion dependent alteration and the centrifugal force field $\omega^2 r$. The evaluation software Sedfit [66] uses numerical finite element solutions to the Lamm equation. This makes it comparably robust with respect to the size range of sedimenting species.

3.2.5 *Enzyme Assays*

MDH activity assay

Mitochondrial malate dehydrogenase (MDH) catalyses the formation of malate from oxaloacetate by simultaneous oxidation of nicotinamide adenine dinucleotide (NADH) as displayed in Equation 3.6.

$$\text{oxaloacetate} + \text{NADH/H}^+ \xrightarrow{\textit{mitoch. MDH}} \text{Malate} + \text{NAD}^+ \tag{3.6}$$

The rate of this reaction is easily followed by the decrease of NADH-absorbance, because NADH and NAD^+ differ in their absorption spectra (see Figures 12): at 340 nm NADH is the only absorbing species.

So by tracing the decrease of absorbance at 340 nm over time, which is proportional to the NADH conversion rate k_{cat}, we compared the activity of known MDH concentrations by Equation 3.7:
(A = absorbance, ϵ_{NADH} = extinction coefficient, d = optical path-length)

$$k_{cat} = -\frac{\Delta[\text{NADH}]}{\Delta t \cdot c_{MDH}} = -\frac{\Delta A}{\Delta t} \cdot \frac{1}{d \cdot \epsilon_{NADH} \cdot c_{MDH}} \tag{3.7}$$

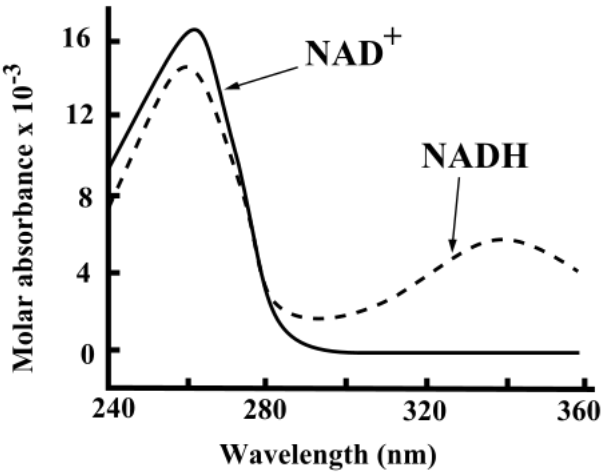

Figure 12: Absorption spectra of NADH and NAD. At 340 nm NADH is the only absorbing species. [14]

By using 0.5 mM oxaloacetate and 0.2 mM NADH in PBS a decent absolute absorbance and no rate limitation by the reactants was observed. A premix was freshly prepared for every experiment.

Aggregation assay

Aggregation of MDH was either provoked by 45 - 60 min incubation at 45°C or through acidic conditions.

The latter was carried out after the approach of Tapley *et al.* [67]. Samples were incubated for 10 min at 37°C in denaturation buffer (150 mM KCl, 150 mM NH_4SO_4, 8 mM H_3PO_4, pH 2) and subsequently neutralized by adding phosphate buffer (pH 8, $V_{buffer} = V_{tot}/10$). Where α-crystallin was added, it was admixed immediately after neutralization.

Aggregation during heat- and acid-denaturation was traced on-line during incubation by recording scattered light. Additionally, heat-denatured samples were also studied by SDS-PAGE. To this end, the samples were centrifuged and the supernatant and the resuspended pellet were analysed.

Refolding assay

This experiments combines the aggregation assay and the MDH activity.

After MDH deactivation during incubation at 45°C for 1 hour, or alternatively, acid deactivation as specified above (10 min at pH 2, 15 min at neutral pH) in the presence of a 2-fold excess of either wild-type or mutant αB-crystallin, the 70/J- chaperone system was added: an ansatz of totally 5 µM Hsc70, 20 µM Hdj1, 2 mM ATP, 5 mM $MgCl_2$ (necessary for ATPase activity), 0.75 µM MDH and 1.5 µM of the respective αB-crystallin in PBS was prepared.

Refolding at 30°C was traced by hourly conducted MDH activity assays.

Regenerative ATPase assay

ATP-hydrolysis by Hsc70 and rate amplification by Hdj1 were analyzed in presence of a regeneration system (Eqations 3.8 - 3.11) to preclude enzymatic inhibition due to product accumulation. Furthermore, the ansatz below provides the cations (Mg^{2+}, K^{+}) necessary for ATPase function (adapted from [68]).

$$ATP + H_2O \xrightarrow{Hsc70} ADP + P_i \tag{3.8}$$

$$PEP + ADP \xrightarrow{PK} Pyruvate + ATP \tag{3.9}$$

$$\underbrace{Pyruvate + NADH/H^{+} \xrightarrow{LDH} Lactate + NAD^{+}} \tag{3.10}$$

$$PEP + NADH/H^{+} \xrightarrow{Total} Lactate + NAD^{+} + P_i \tag{3.11}$$

Final concentrations were 150 mM KCl, 50 mM HEPES/KOH, 10 mM $MgCl_2$, 1mM ATP, 2 mM Phosphoenol pyruvate (PEP), 0.2 mM NADH, 2 U/ml pyruvate kinase (PK), 10 U/ml lactate dehydrogenase (LDH), 15 mM $(NH_4)_2SO_4$. A baseline was recorded at 340 nm and the reaction was started by adding varied concentration of Hsc70 and Hdj1.

Assessment of the hydrolysis rate was analogue to MDH activity evaluation (see Equation 3.7).

Ellman's assay

The number of accessible cysteines incorporated in MDH were quantified by the Ellman's assay, for labeling reasons. It can be quantified by letting the *Ellman's reagent*, 5,5'-dithio-bis-nitrobenzoic acid (DTNB) react with free thiols as shown in Equation 3.12. The resulting 2-nitro-5-thiobenzoate has an absorption maximum at 412 nm, as soon as it is ionized [69].

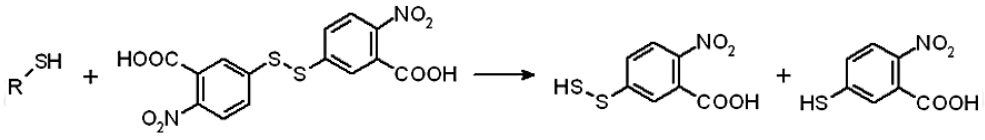

(3.12)

The following ansatz was prepared: 25 mM sodium acetate, 1 mM DTNB and 100 mM Tris in 990 µl nano-pure water. After acquiring a baseline scan from 250 to 450 nm, 10 µl of 120 µM MDH were added. Following 5 min of incubation at 20°C, the spectra was captured again.

The number of free cysteins, x_{Cys}, is then determined after Equation 3.13:
absorbance A, optical path-length d, extinction coefficient $\epsilon_{NTB^{2-}} = 14150\,M^{-1}\,cm^{-1}$ (in dilute buffers [70]), initial MDH concentration c_{MDH}, dilution factor $f_{dilution}$.

$$x_{Cys} = \frac{c_{Cys}}{c_{MDH}} = \frac{A_{412}/d/\epsilon_{DTNB}}{c_{MDH}} \cdot f_{dilution} \tag{3.13}$$

4

RESULTS & DISCUSSION

4.1 CLONING

All the combinations of the mutation sites at residues 19, 45, 59 were cloned (see Table 19). As a first assessment, the size of every PCR product was examined by agarose gels. The respective gels are found in the Appendix A.2). In the end, sequencing results from *GATC Biotech AG* (Konstanz, Germany) gave certainty about the cloned construct.

Beyond those, the wild-type protein, αB-3E and αB-A4C-3E were expressed and purified.

Table 19: The αB_{WT}-template and the cloned mutants. Only the N-terminal 60 residues are displayed. The remaining fragment is identical for all constructs.

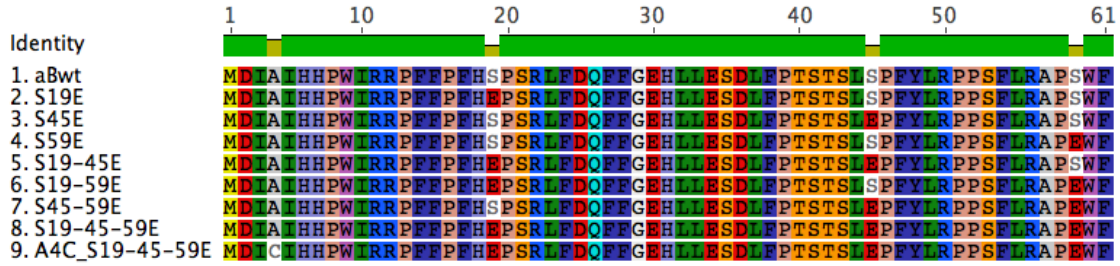

4.2 PROTEIN PURIFICATION

4.2.1 αB-crystallin

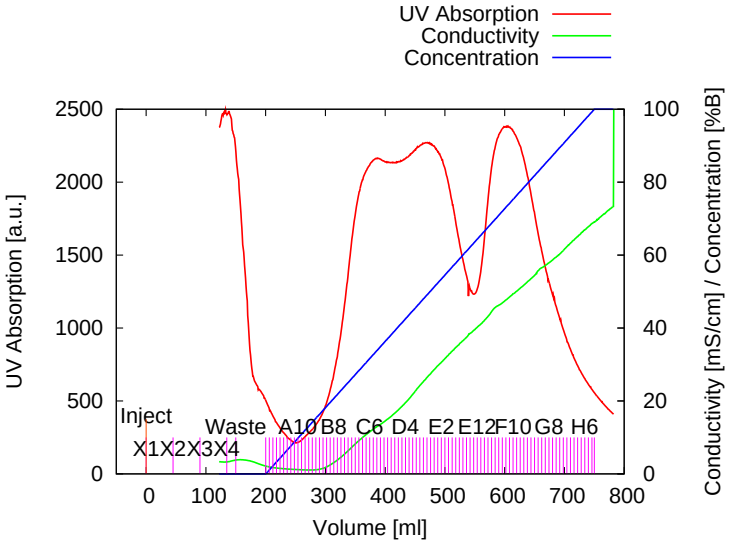

Figure 13: Chromatogram and resulting SDS-gel of anion exchange chromatography performed with a self-packed *Q Sepharose* column. In the chromatogram, the indicated fractions are displayed in pink. Fractions B1 to C12 were pooled for further purification.

In the following, we illustrate the purification of αB-crystallin on the basis of the αB_{WT} purification, which is representative for the purification of the αB-mutants, too. The remaining gels of αB_{WT}, as well as gels and chromatograms of αB-3E and αB-A4C-3E purification, are found in the Appendix A.3.

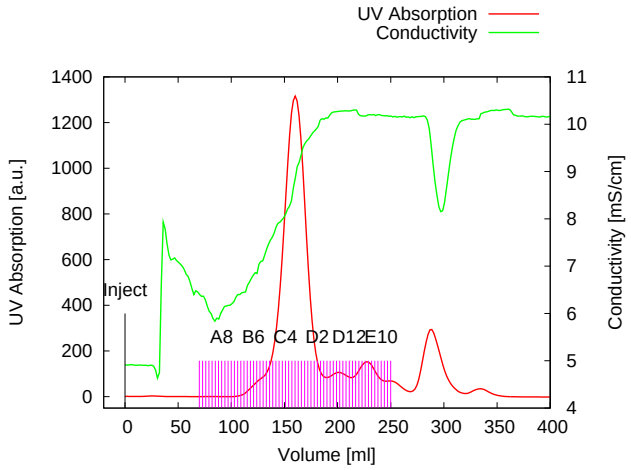

Figure 14: Chromatogram and resulting SDS-gel of size exclusion chromatography performed with a *Superdex 200* column. In the chromatogram, the indicated fractions are displayed in pink. Pooled for further purification were fractions B11 to C11.

The first purification step was anion exchange chromatography. A self-packed *Q Sepharose* column was utilized for this purpose. The salt gradient applied for protein elution along with the absorption profile is shown in the chromatogram, Figure 13. Inspection of the resulting SDS-gel led to a pool of fractions B1 to C12 (elution at 100 - 350 mM NaCl), which was reconcentrated and further purified.

As a second step, size exclusion chromatography was performed using a *Superdex 200* gel filtration column. This produced the elution profile displayed in Figure 14. The pooled fractions were A5 - A10.

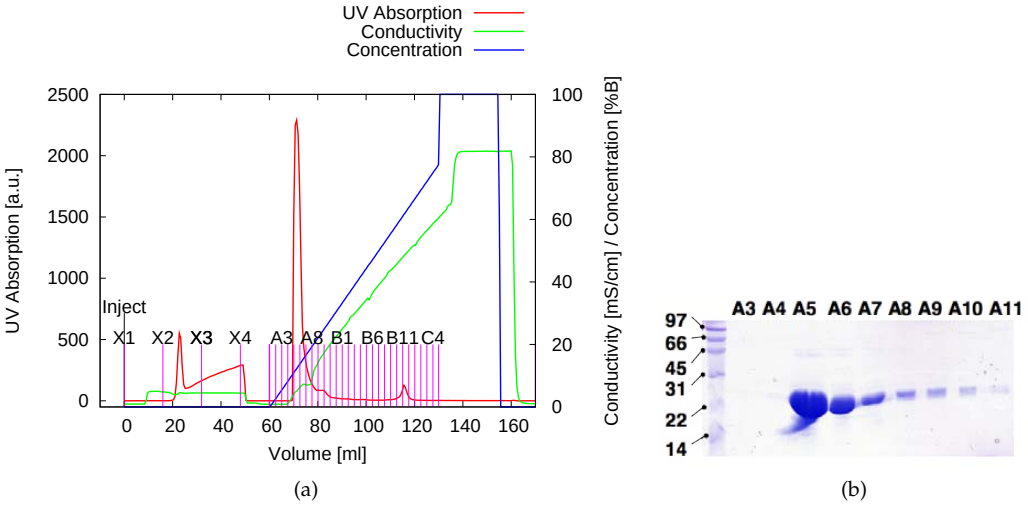

(a) (b)

Figure 15: Chromatogram and resulting SDS-gel of anion exchange chromatography performed with a *Resource Q* column. In the chromatogram, the indicated fractions are displayed in pink. Molecular weights of the SDS-PAGE marker proteins are specified in kDa. Fractions A5 to A10 constitute the final yield.

Following dialysis in salt-free buffer, the protein was subjected to another AEC employing a *Resource Q* column. At 100 mM NaCl, αB_{WT} eluted as displayed in the chromatogram, Figure 15a). The purity of αB_{WT} was confirmed by SDS-PAGE (Figure 15b, $M_W(\alpha B)$ = 20 kDa). Fractions A5 to A10 were dialyzed against PBS and reconcentrated to 10 mg/ml. The total yield of wild-type αB-crystalline was 110 mg from a 7.5 l *E.coli* culture.

4.2.2 *Human DnaJ homologue (Hdj1)*

The purification of Hdj1 was initiated by cation exchange chromatography using an *SP Sepahrose* column. Applying a linear salt gradient, the protein eluted at 200 - 250 mM NaCl (cf. Figure 16). Following the result of the SDS-gel, fractions B9 to C1 were pooled and reconcentrated.

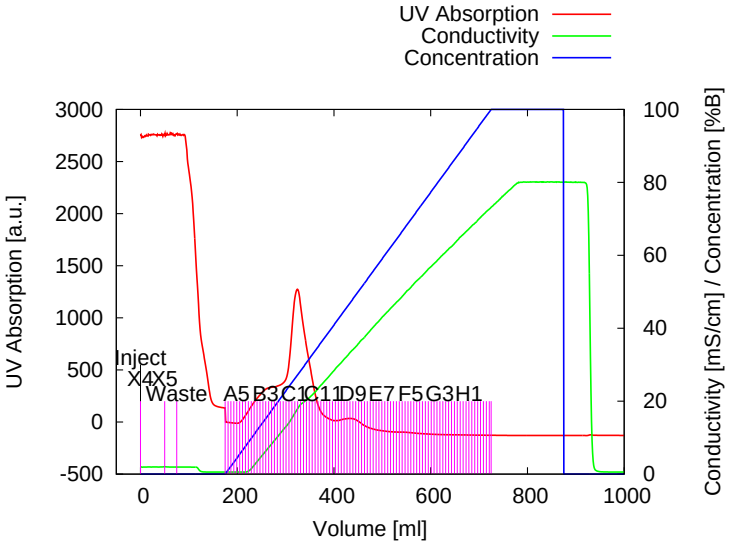

Figure 16: Chromatogram of cation exchange chromatography. Collected fractions are displayed in pink. The resulting pool consisted of fractions B9 to C1.

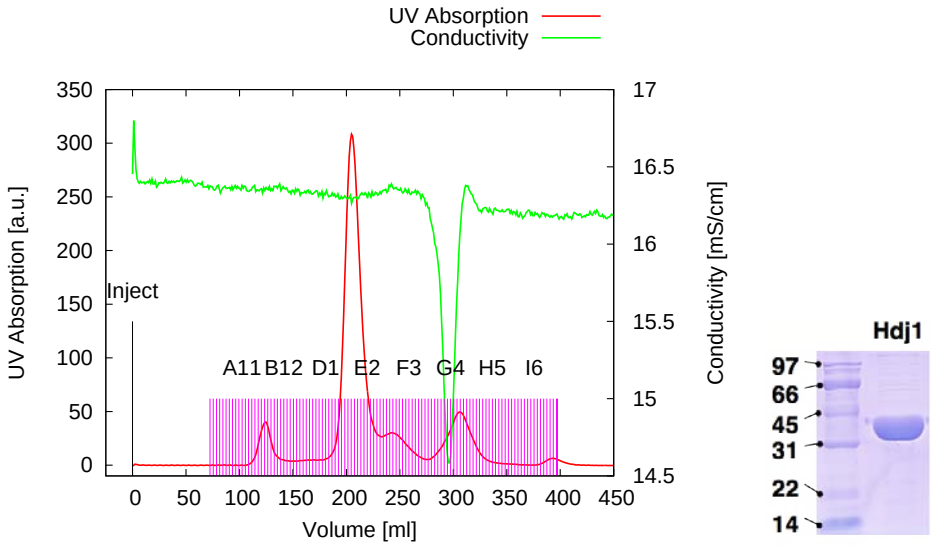

(a) (b)

Figure 17: 17a Chromatogram of size exclusion chromatography. Collected fractions are displayed in pink. Pure Hdj1 was collected in fractions D6 - E5. 17b SDS-gel of purified Hdj1. Molecular weights of the marker proteins are specified in kDa.

The second purification step was size exclusion chromatography applying a *Superdex 200* gel filtration column. As shown in the chromatogram, Figure 17a, Hdj1 was collected in fractions D6 - E5.

The SDS-gel (Figure 17b) revealed pure Hdj1 (M_W = 38 kDa) after two chromatographic procedures. It was dialyzed in PBS and reconcentrated to ca. 2 mg/ml. The total yield of human DnaJ homologue was approximately 50 mg from a 7.5 l *E.coli* culture.

4.3 AUXILIARY ENZYMATIC ASSAYS

4.3.1 *MDH Activity Assay*

After testing citrate synthase, luciferase and lysozyme, malate dehydrogenase was chosen as a model substrate, because its activity is easily traced by NADH absorption as explained in the methods, Section 3.2.5. This is very helpful for characterizing substrate deactivation or reactivation in refolding assays. In contrast to assays that are based on secondary effects, such as changes in intrinsic fluorescence, the MDH activity assay provides the possibility to really assess regained *enzymatic function*.

Since MDH activity served as a rule, its standard turn-over number was determined as a reference. Figure 18 shows the raw data of MDH activity assays (left) carried out with indicated MDH concentrations, 0.5 mM oxaloacetate and 0.2 mM NADH. A first phase of constant enzymatic activity is followed by a gradual activity drop caused by substrate limitation.

The slope values obtained by fitting the linear section are shown on the right hand side. Application of Equation 3.7 gave a turn-over number of 71.0 ± 7 s^{-1}, which fits well with the literature value of 76.7 s^{-1} [71].

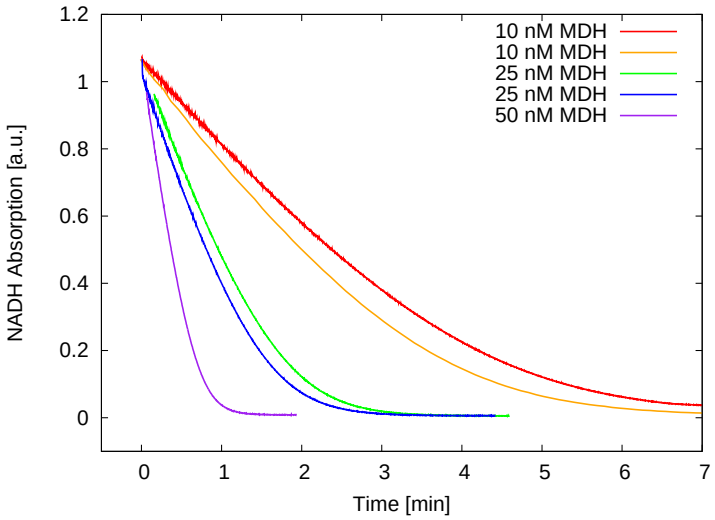

Concentration [nM] :	k_{cat} [s^{-1}]
10	67.2
10	75.8
25	73.3
25	64.2
50	74.5
Average k_{cat} [s^{-1}] :	71.0 ± 7

Figure 18: The MDH activity assay (left) with indicated MDH concentration resulted in the slopes (right), from which an average MDH activity of 71.0 ± 7 s^{-1} was deduced.

4.3.2 *Hsc70 ATPase Assay*

The preferential conditions for the chaperone system, consisting of human Hsc70 and Hdj1, were examined by the following ATPase assay.

At first, the temperature dependence of the ATPase activity was analysed. Figure 19a shows that Hsc70 is tolerant to 30°C also *in vitro*, and its activity was 1.5-times higher than at 20°C.

By varying the concentrations of ATPase assistant Hdj1, we found that the Hsc70 hydrolysis rate doubled when a four fold excess of Hdj1 was applied (see Figure 19b). A turn-over number of 0.23 ATP molecules per minute was deduced in this case, whereas the literature value lies at 0.15 molecules / min measured at 37°C without co-chaperone [72].

Consequently, the refolding assays were set up according to these findings, i.e., a 1:4 ratio of Hsc70 and Hdj1 concentrations at 30°C.

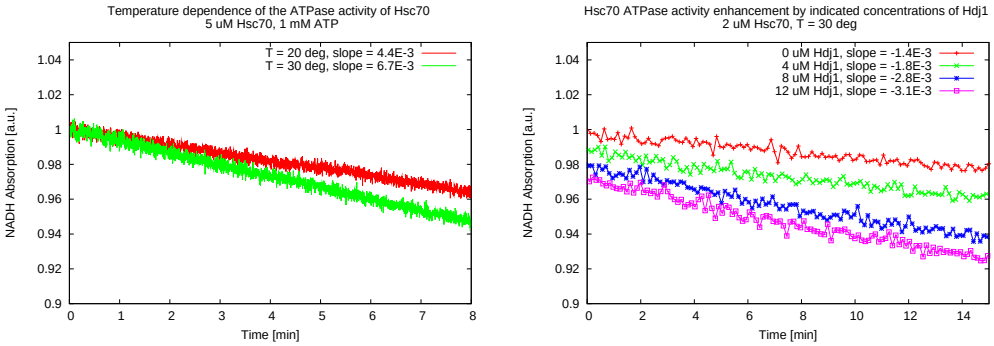

(a) (b)

Figure 19: ATPase assay of 5 µM Hsc70 at 20 and 30°C (a). Hdj1 titration of 2 µM Hsc70 at 30°C.

4.3.3 *Ellman's Assay*

An Ellman's assay was performed on MDH to assess the number of accessible cysteines (see Figure 20). An average NTB^{2-} absorbance of 0.075 a.u. was obtained, which (by Equation 3.13) amounts to four accessible cysteines per MDH molecule. Thus, fluorescent MDH labeling by thiol coupling is feasible.

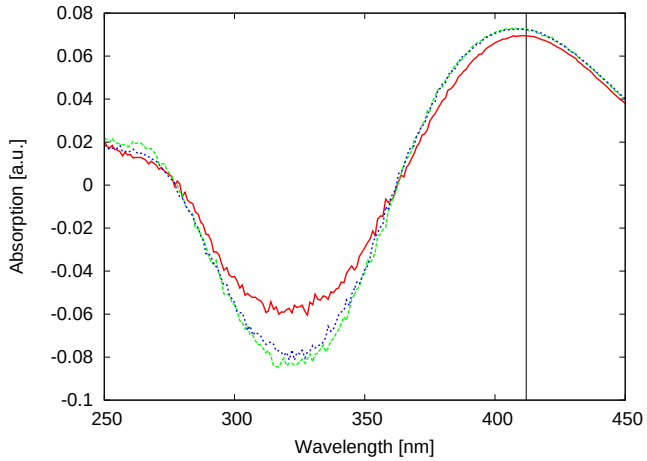

Figure 20: Ellman's assay of MDH. Absorbance at 412 nm = 0.0715, which matches 4 cysteins.

4.4 PROTEIN CHARACTERIZATION

4.4.1 *Primary Structure*

Additionally to the information of SDS-PAGE, mass spectroscopy was carried out to conclusively identify the protein. The spectra were acquired by Helmut Krause at a MALDI-TOF mass spectrometer. The spectra in Figure 21 show distinct peaks at the complete, one half and / or one-third of the respective molecular masses corresponding to 1, 2 or 3-fold charged species.

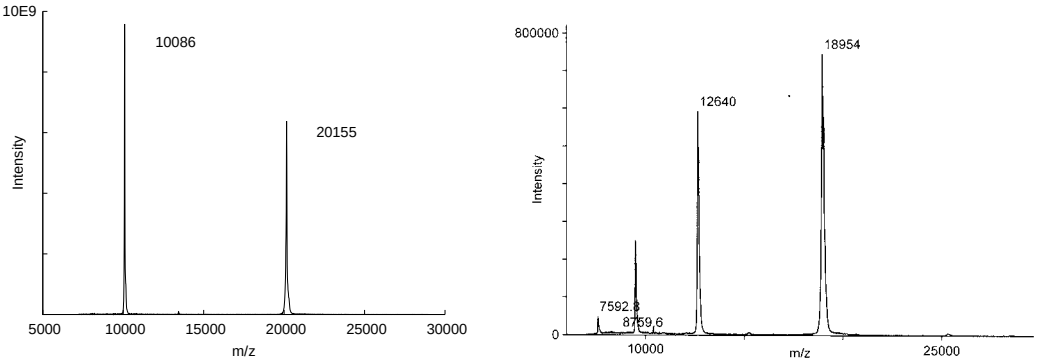

(a) (b)

Figure 21: (a) Mass spectrum of purified αB_{WT} (M_W = 20158 Da). The singly and 2-fold charged peaks are visible. (b) In the Hdj1 spectrum (M_W = 38044 Da) the 2- and 3-fold charged peaks were detected.

4.4.2 *Secondary Structure*

The content of α-helices and β-sheets was studied by CD-spectroscopy:

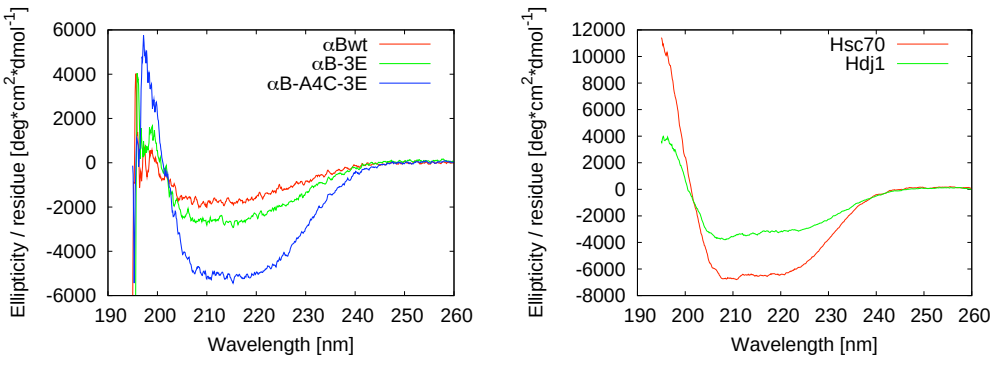

(a) (b)

Figure 22: CD-spectra of the three αB-derivates (0.1 mg/ml) (a), and of Hsc70 and Hdj1 (0.2 mg/ml) (b) all acquired at 20°C.

Figure 22a compares the indicated αB-mutants. All curves share a negative band centered at 215 nm, which is characteristic for β-sheets. This is congruent with the known high β-sheet content present in the α-crystallin domain (cf. Figure 23a). However, this negative band reaches from below 210 nm up to above 222 nm, which implies some superposed α-helical character. Yet, the extinction is comparably small for α-helices indicating a very low α-helical content.

If the differences *between* the three variants represents a real secondary structural difference, or if it is rather due to slightly differing concentrations, can not be elucidated by this method alone. The additional cysteine in αB-A4C-3E could be involved in the difference, too. Although cysteines principally absorb at 250 nm.

Finally, the noise around 195 nm is most certainly attributable to buffer components absorbing below 197 nm.

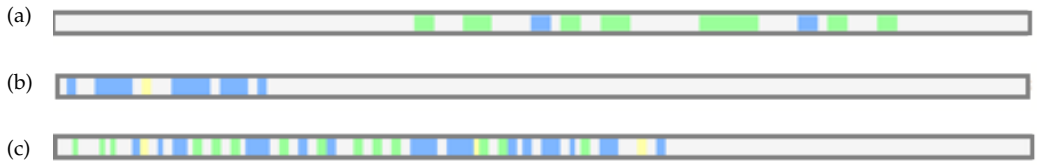

Figure 23: Secondary structure assignment to human αB-crystallin, Hdj1 and Hsc70. Blue: α-helices, green: β-sheets, yellow: loops. Retrieved from *UniProtKB* [15].

In the second spectrum, Figure 22b, the α-helical bands at 208 nm and fainter around 222 nm can be discerned for both proteins. Together with the high positive peak at 195 nm, this is indicative for a predominantly α-helical character, which is in good agreement with the domain assignment found in literature (cf. Figure 23).

4.4.3 *Quaternary Structure*

HPLC was performed to gain insight into the oligomeric assembly of αB-crystallin. Figure 24a shows the chromatogram of αB_{WT}, αB-3E and αB-A4C-3E. The data was acquired using a *TSK* gel filtration column, which was calibrated as specified by Figure 24b.

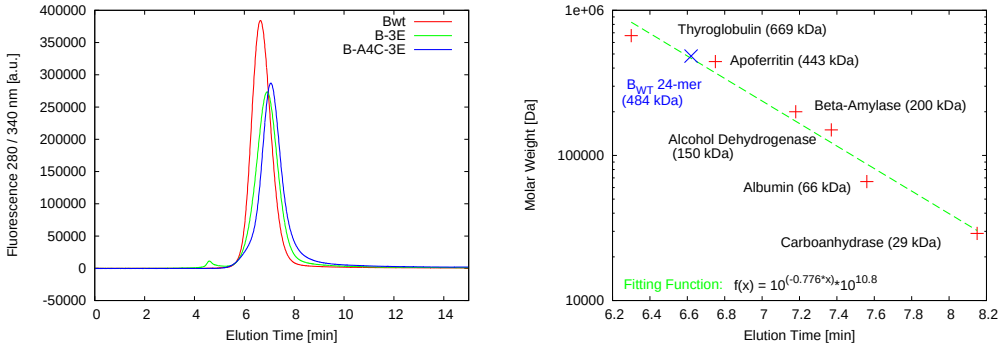

(a) (b)

Figure 24: HPLC results of the indicated three αB variants (a). A *TSK* gel filtration column was employed at 20°C. (b) shows the calibration line fitted from the indicated reference proteins. The αB_{WT}-24-mer complex aligns nicely with the calibration line.

αB_{WT}, αB-3E and αB-A4C-3E eluted after 6.6, 6.8 and 7.0 min ± 0.01 min, respectively. Applying the deduced fitting function, yields for the wild-type a 477 kDa complex, which fits quite well to the 480 kDa of the 24-mer found in literature [7].

On the other hand, the triple-E mutants feature lower oligomeric species of 12 - 16 subunits. This is in agreement with results from literature saying that phosphorylation leads to smaller multi-meric complexes [50], [5], [51].

4.5 SUBSTRATE PROTECTION AGAINST AGGREGATION

Small heat-shock proteins are known to suppress aggregation of their substrates. In this respect, several *in vivo* studies showed an altered effect of phospho-mimetic mutants as explained in the introductory section 1.1.

Furthermore, phosphorylated αB-crystallin was found in *in vivo* studies. Therefore, it was interesting to see the effect of mimicked phosphorylation at three positions in comparison with the αB wild-type.

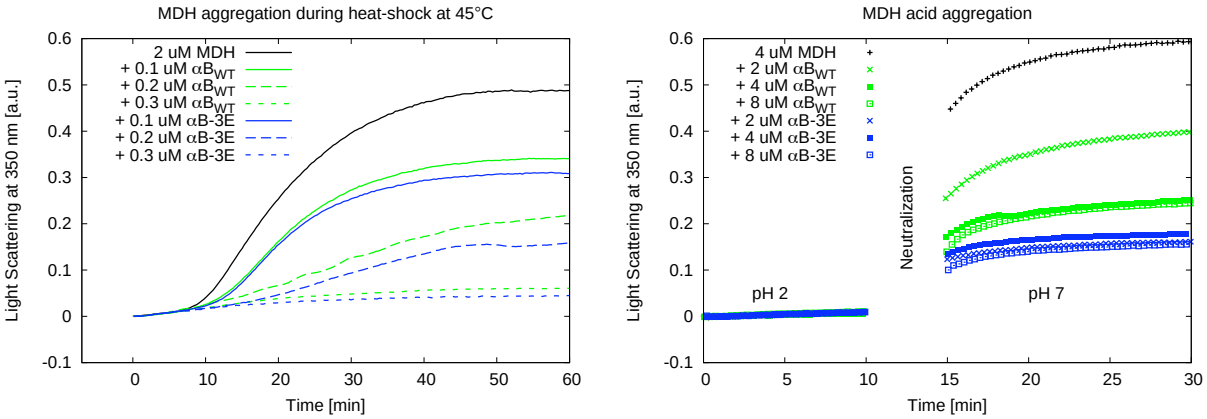

Figure 25: Representative results of aggregation assays applying heat (left) or acidic (right) conditions to enforce unfolding of MDH.

In this regard, we conducted aggregation assays. Figure 25 includes representative results of both alternative approaches: unfolding due to heat (left) and acidic conditions (right). It is apparent that the most light-scattering MDH aggregates precipitated, when MDH was incubated without any α-crystallin. So, both experiments reveal αB-crystallins' ability to suppress aggregation.

The most interesting result, however, is that αB-3E is reproducibly more active than the wild-type - in both experiments. The question, if this effect is related to the previously found differing oligomeric species, is addressed in the next section.

But first the above data shall be confirmed by a second analytical technique: SDS-PAGE. Thereby, doubts about possible sinking of heavy aggregates during the time of the experiment are resolved.

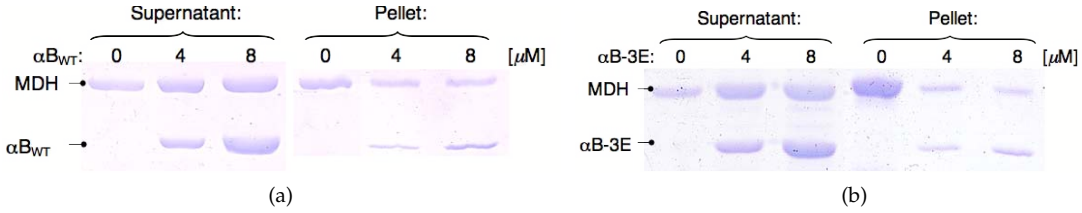

Figure 26: SDS-PAGE analysis of the soluble and precipitating fraction. 5 μM MDH were incubated with the indicated concentrations of either αB_{WT} or the αB-3E.

Additionally, this offers a closer look at the soluble fraction, which is not considered in the above LS detection method. Figure 26 shows that with increasing concentration of α-crystallin, not only the amount of aggregates decreases, but there is really more MDH kept soluble. The

quantitative difference between wild-type and mutant is yet more difficult to demonstrate by this method.

4.6 αB - SUBSTRATE COMPLEXES

To further investigate the differences and similarities of αB wild-type and triple-E mutant, the substrate complexes were investigated by HPLC. Again, binding was initiated by heat (45°C). The chromatogram of the soluble fraction after different incubation times is displayed in Figure 27. Table 20 contains the elution time together with the deduced masses of the studied complexes.

Remarkably, the MDH peak vanishes after the first few minutes of heat incubation. This means that already after 30 min at 45°C there is practically no free, soluble MDH present anymore. Either it is bound or it has precipitated.

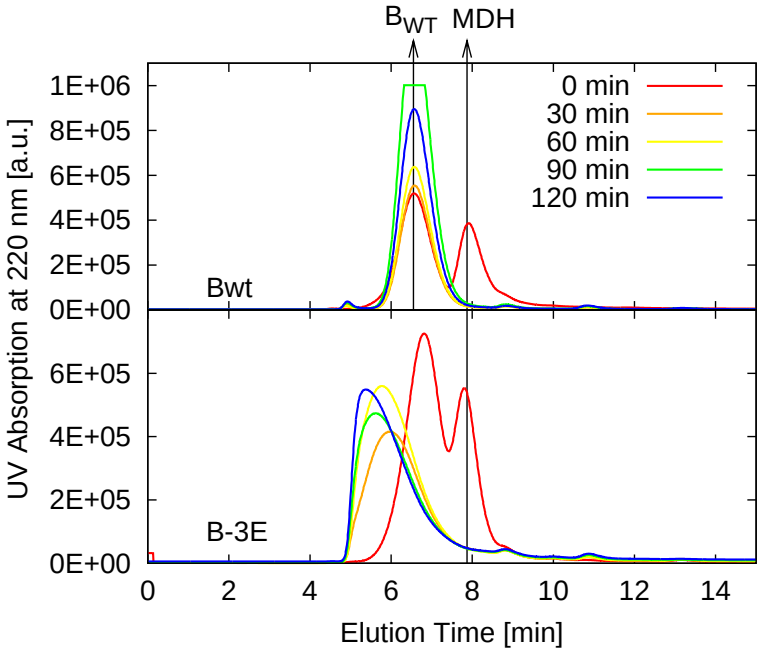

Figure 27: HPLC chromatograms of 24 μM αB-crystallin and 10 μM MDH as specified. Samples were incubated for the specified periods at 45°C before measurement.

Table 20: Elution times and deduced masses of the complexes studied by HPLC.

Protein:	elution time [min]:	deduced mass [kDa]:
αB_{WT}	6.6	477
αB_{WT} + MDH	6.6	477
αB-3E	6.8	328
αB-3E + MDH	6.0 - 5.4	1390 - 4070

The upper half of Figure 27, however, shows that αB_{WT} has not bound any substrate: the peaks are precisely aligned at the position of the 24-mer. This is in contradiction to the results of the aggregation assays, where a clear interaction between αB_{WT} and MDH was found.

Things are different for the mutant: here, the shifts in elution time, due to substrate binding, are unmistakeable. Even after 90 min incubation time, no saturation came about. Yet more substrate is being bound. Although, the column calibration may not be very precise in the range of these large complexes, the observed elution times indicate that multiple MDH molecules are bound per αB-3E subunit.

One might argue that there is probably some interaction with the gel filtration matrix, and that the lack of binding of the wild-type is simply an artifact. To exclude this, we analyzed the same species by analytical ultra-centrifugation.

But the results in Figure 28 support those obtained by HPLC: there is an indisputable difference between wild-type and mutant. One single peak is found for the former, whereas αB-3E alone exhibits two oligomeric species (red lines, without substrate). Knowing that the αB_{WT} peak reflects the 24-mer, the triple-E mutant occurs partly as a 24-mer, too, but the prevailing species is a slightly smaller oligomer.

The 24-mer of αB-3E was not detectable by HPLC. This implies that, in contrast to the wild-type, the mutant complex could not resist the shearing forces occurring during gel filtration. Therefore, lower *inter-subunit* affinities are assumed.

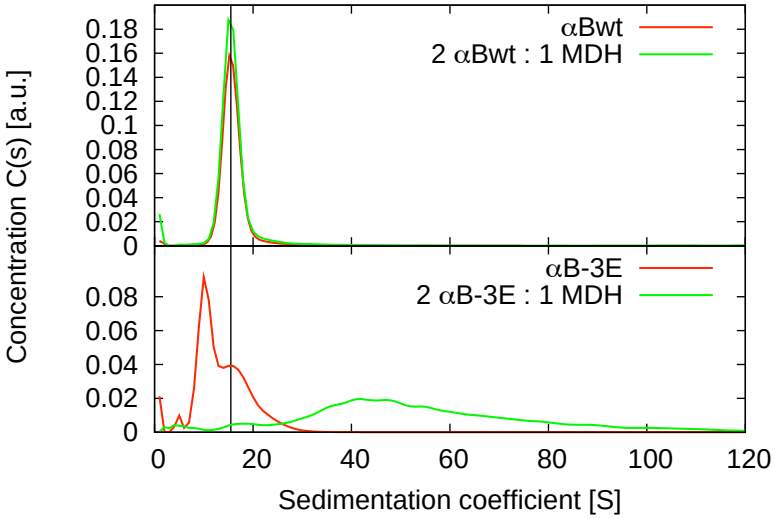

Figure 28: Concentration distribution with respect to sedimentation deduced form AUC sedimentation velocity experiments. Concentrations were 43 µM for αB-crystallin and 21.5 µM MDH giving rise to total absorbances of 0.7 to 0.9 per sample (optical path-length = 1.2 cm).

In agreement with HPLC, no αB_{WT}-substrate complexes could be detected in Figure 28, whereas the mutant seems to form complexes of diverse composition stoichiometries.

4.7 SUBSTRATE BINDING & RELEASE

Substrate binding of wild-type αB could not be confirmed by FRET. Figure 29 shows that no energy transfer was detected. Whereas the donor fluorescence remains constant throughout the measurement, the increase of acceptor fluorescence, reflects aggregation of MDH: quenching by solvent interactions is suppressed because the fluorescent dye co-aggregates with the protein. This supports the results of HPLC and AUC, but it is in contrast to the aggregation assays.

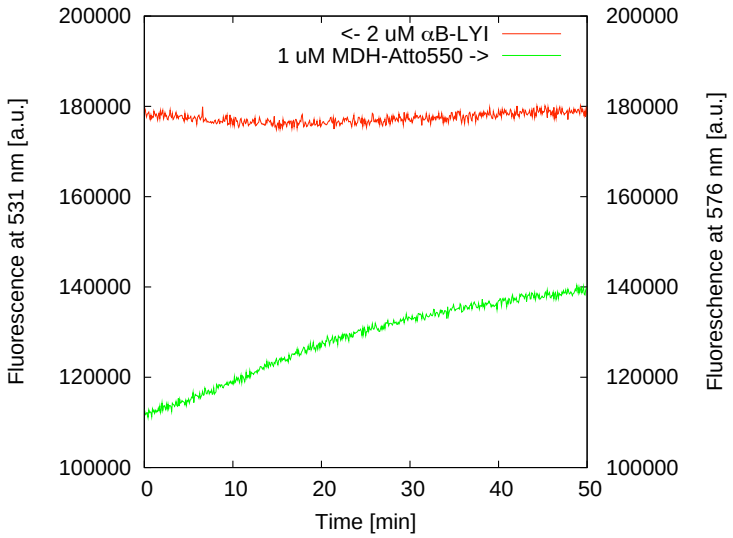

Figure 29: Measurement of donor (αB_{WT}-LYI) and acceptor (MDH-Atto550) fluorescence as indicated. No FRET system is established.

Although, the foregoing experiments suggest substrate binding by phospho-mimetic αB, this could not be implemented within the scope of this thesis.

4.8 SUBSTRATE REACTIVATION

To complete the circle, MDH was not only subjected to aggregation, but it was subsequently supplied with refolding agents (Hsc70, Hdj1) to recover its activity. Figure 30 displays raw data of a typical experiment.

It is apparent that the amount of regained activity depends on the conditions during heat or acid deactivation: if no α-crystallin is present (black lines), basically no MDH activity is found even after a refolding time of 5 hours.

If, however, αB-crystallin is present during deactivation, it can bind unfolding intermediates, thus, retrieving the substrates from their pathway towards aggregation (cf. Section 4.5). Only if the substrate remains soluble, the chaperone system can cope with the unfolding intermediate and promote its refolding, later on. Thereby, we observed better reactivation yields with αB-3E as compared to αB_{WT}.

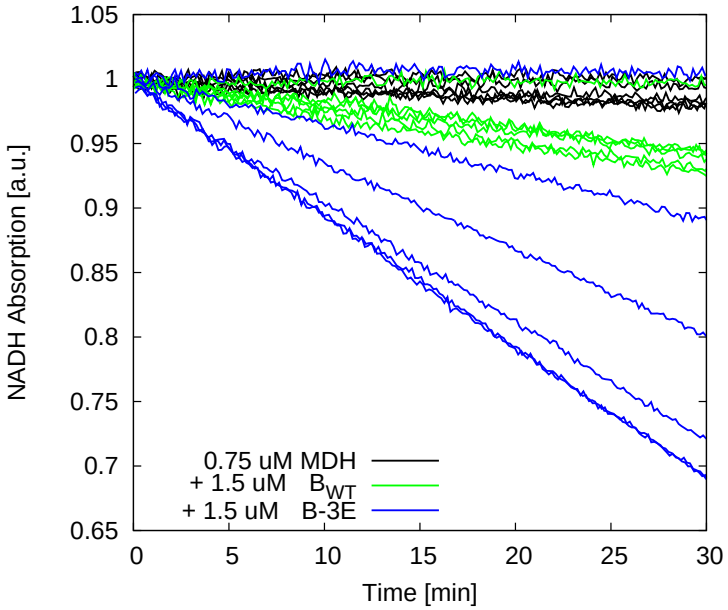

Figure 30: Outline of MDH reactivation over time, after heat or acid deactivation with the indicated proteins. Data was measured at 20°C after 1 to 5 hours of incubation at 30°C in presence of 5 µM Hsc70, 20 µM Hdj1 and 2 mM ATP. A representative of three identical experiments is shown.

4.8.1 *Wild-type vs. Mutant*

As mentioned before, αB-3E has allowed for better MDH reactivation as compared to the wild-type. A more than 5-times increased quota was detected in the first case. This is illustrated by Figure 31, which contrasts the experimentally recovered MDH activity, with the actual activity of the MDH concentration present in the system.

These findings imply that although, previous results indicate an increased substrate complex stability for the phospho-mutant, substrate release by αB-3E is not rate limiting in substrate reactivation. Substrate refolding by Hsc70 is apparently not perturbed by a higher affinity of αB-3E. Rather the initial substrate binding step during denaturing conditions seems crucial for later reactivation.

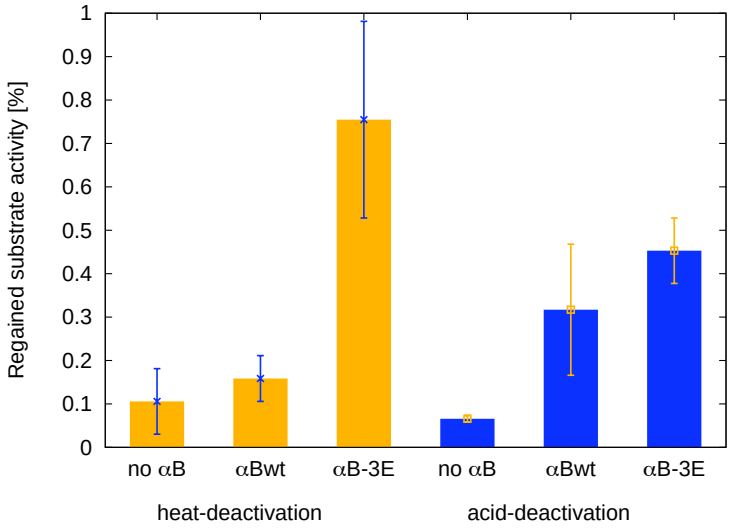

Figure 31: Evaluation of three refolding experiments following either heat or acid deactivation. Error-bars represent largest absolute errors.

Whereas the contrast between mutant and wild-type is quite pronounced after heat-deactivation, the difference is less explicit for refold following acid deactivation. A reason for this may be the shorter unfolding time (15 min after neutralization as compared to 60 min at 45°C). If the difference between both αB-crystallin variants lies really in their differing substrate complex stability, then - for thermo-dynamic reasons - the difference in substrate activity regain becomes larger, the longer period is spent under denaturing conditions.

Additionally, the graphic reveals the aforementioned low percentage of reactivated MDH: less then 1 % of the initial MDH concentration could really be recovered. Potential optimizations are discussed in the next section.

4.8.2 *The Reactivation Process*

Unfortunately, there is no kinetic model, so far, which describes the set of reactions taking place in the reactivation framework. So, assessing the time-course of substrate refolding was difficult.

Equations 4.1 to 4.5 list involved processes: aggregation prone substrates are bound at the level of the unfolding intermediate (4.1) by an activated form of αB-crystallin (4.2). Thereby a substrate complex forms (4.3) that is capable of keeping the partially unfolded substrate soluble. This is a prerequisite for later binding to Hsc70 (4.4), and thus, for substrate refolding in general (4.5).

$$[S]_{native} \xrightarrow{\text{unfolding}} [S]_{intermediate} \xrightarrow{\text{further unfolding}} [S]_{aggregate} \tag{4.1}$$

$$[\alpha B]_{storage} \xrightarrow{\text{heat/acidic stress}} [\alpha B]_{active} \tag{4.2}$$

$$[S]_{intermediate} + [\alpha B]_{active} \xrightarrow{\text{binding}} [S\text{-}\alpha B] \tag{4.3}$$

$$[S\text{-}\alpha B] + [Hdj1] + [Hsc70\text{-}ATP] \xrightarrow{\text{pass over}} [\alpha B] + [Hdj1] + [S\text{-}Hsc70\text{-}ADP] \tag{4.4}$$

$$[S\text{-}Hsc70\text{-}ADP\text{-}Hdj1] + [ATP] \xrightarrow{\text{chaperone function}} [S]_{native} + [Hsc70\text{-}ATP] + [Hdj1] + [ADP] \tag{4.5}$$

Among these processes, many steps are not entirely understood, yet:

There is, for instance, still a debate about the oligomeric state of really *active* αB-crystalline. Our HPLC and AUC results (see αB-3E data in Figures 27 and 28 where binding was observed) indicate that rather 12-mer than 24-mers or dimers constitute the actually binding species. This is supported by other groups' results [5] which suggest further that these smaller multimeric complexes comprise a high-capacity - but low-affinity - mode resulting in large substrate complexes. Whereas the large substrate complexes were also observed in the present work, at least some complexes, within the broad distribution found by AUC, show sufficient substrate affinity to sustain HPLC.

The high-capacity state may be favored in our experiments, because of an excess of sHsp over substrate, and because the substrate is already present during αB activation. Thus, the activation process of αB-crystallin must be temporally correlated with substrate unfolding for any *binding* to take place. Under these circumstances, αB oligomers may be loaded with substrate *before* transformation into the high-affinity state occurrs. On the other hand, pre-incubation of αB-crystallin alone, at elevated temperatures may reveal the high-affinity state [73].

Additionally, the so-called *passing-over* reaction (Equation 4.3) has not been elucidated, yet. How does release of the substrate-αB-complex happen? Following the hypothesis of *active* and *passive* forms, αB might be reconverted into its higher oligomeric storage state after the stress period, and thus, release its substrate spontaneously. On the other hand, the action of Hdj1 *grabbing* unfolded stretches of the substrate and thereby enforcing release from αB would be conceivable, too.

Finally, there are still obscure parts in the actual chaperone function of the 70/J - system: Is the refolding activity of Hsc70 proportional to its ATPase activity? Meaning, is it possible at all, to amplify the refolding capability by optimizing the hydrolysis rate? Namely in the case of Hsp90, a direct relation between ATPase activity and conformational changes - needed for chaperone function - has been disproved [22]. Preliminary results of ours also imply that by applying lower amounts of Hdj1, the amount of reactivated MDH was higher. Furthermore, there is a second human J-domain protein that might increase the refolding yields. Also, the nucleotide exchange factor, Bag1 (cf. Section 1.2), has not been employed herein. Comparison with similar experiments, found in the literature, shows that a chaperonin system is often applied in combination with the Hsc70-Hdj1-Bag1 analogue of *E.coli* [18][55]. Additionally, an ATP regeneration system, comparable to the one applied for the ATPase assays herein, was used in published experiments [30]. This could be a hint of possible product inhibition of the ATPase by ADP in our experiments.

Although the mathematical background lacks almost completely, we found that a lognormal fit emulates the experimentally observed reactivation process - which includes reactions 4.1 to 4.5 - at least qualitatively (see Figure 32). Upon addition of Hsc70 / Hdj1 at t = 0, an initial lag phase of about 1 hour was observed before reactivation became measurable. Following rapid reactivation during the second hour, a maximum of recovered MDH activity was measured after 4 hours of refold before the observed activity decreased again.

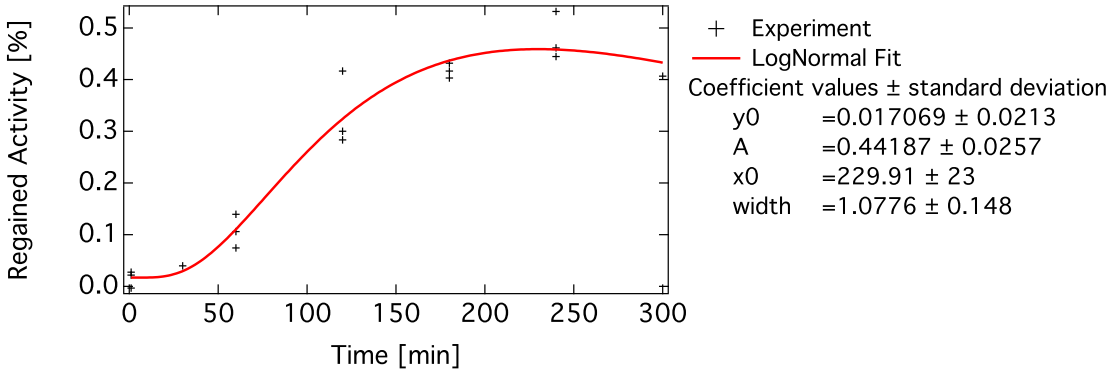

Figure 32: Time course of the refolding reaction after acid induced MDH unfolding in the presence of αB-3E. Time-resolved reactivation data of three equivalent experiments (black) was fit with a lognormal function (red): $f(x) = Y0 + A \cdot exp[-(\ln(x/X0)/width)^2]$

4.9 ENSEMBLE DISCUSSION OF RESULTS

Seemingly, there is a contradiction within the data presented herein: on the one hand, an aggregation suppressive effect of wild-type αB-crystallin has been measured by two separate approaches in Section 4.5. On the other hand, an αB_{WT} - substrate interaction could not be detected by any other method applied, including FRET, AUC, HPLC.

FRET experiments may be hindered by the label molecule: since substrate binding occurs by unspecific, unpolar interactions, no concrete binding site has been discerned, yet. Thus, interference of the label in the binding process can not be excluded. Furthermore, the stability of the fluorescent label at denaturing conditions is not guaranteed. Concerning HPLC, surface interaction or shearing due to the stationary phase may cause complex dissociation. And AUC measurements may last too long for the substrate complexes to stay bound.

Nevertheless, this differences in substrate complex stability are clearly a contrast between wild-type and αB-3E. As mentioned before, this is indicative of a lower substrate complex stability in the un-phosphorylated form of αB.

Additionally, we found differences in αB *oligomer* stability. Whereas αB_{WT} 24-mer was identified by HPLC, it was not observed in the case of αB-3E. Only AUC could uncover this species together with a second smaller oligomer. The smaller about 10 to 14-meric αB-3E complexes were described before by other groups, who proposed the decay into smaller oligomers during stress to be related with the activation process of phosphorylated αB [5].

Since the interaction of αB-crystallin with its substrate is of hydrophobic nature, and occurs possibly at multiple positions within one subunit, as well as between several neighboring subunits, the idea of the volume to surface ratio suggests itself: by splitting a spherical complex ($A = 4\pi r^2$) into 2 halves ($A = 2 \cdot (2\pi r^2 + \pi r^2)$), the totally exposed surface increases by a factor of 1.5 (if no further subunit rearrangements are assumed). Thereby, new surfaces become accessible for substrates, namely the subunit-subunit contact sites. This explains the different substrate complex stabilities for wild-type and phosphorylated αB: with the dissociation into smaller multi-mers, more affine binding sites (formerly covered by inter-subunit contacts) become exposed. Thus, this reasoning relates the decreased complex size and stability of the triple-E mutant, to the increased substrate binding capacity, in contrast to the wild-type.

In that sense, phosphorylation of αB can be understood as a means of activation that intensifies substrate interactions. Whereas such higher αB reactivity may be beneficial to a cell under stress conditions, it is very likely that a constant high level of post-translationally phosphorylated αB results in a constant *on-state* of the αB high-affinity mode. In the absence of stress, this could be pathogenic because further binding of *native* substrates, too, would result in αB induced unfolding of the substrates, along with uncontrolled aggregation. Such pathologic effects originating from a gain of function are reminiscent of the introduced aggregation related diseases (cf. Section 1.1).

5

CONCLUSION & OUTLOOK

5.1 CONCLUSION

Within this master thesis, 9 αB mutants were cloned, αB_{WT}, two phospho-mimetic αB mutants (αB-S19-45-59E, αB-A4C-S19-45-59E) and Hdj1 were expressed recombinantly in *E.coli*, and the target proteins were purified at good yields.

The acquired proteins were analyzed by protein-chemical, as well as spectroscopic and chromatographic methods. The obtained results were comparable to literature values.

The oligomerization state of αB was further studied by AUC. Combining the results of HPLC and AUC, we deduced a 24-meric complex as the prevailing αB_{WT} species at 20°C and 45°C. For the phospho-mimetic αB variant, however, a combination of two species was found: a 24-mer of low stability and a smaller oligomer of 10 to 14 subunits.

Whereas substrate binding of wild-type αB could not be shown by *direct* methods (i.e. FRET, HPLC, AUC), a broad distribution of large substrate complexes was found for phospho-mimicking αB-3E. Among the different substrate complex stoichiometries observed by AUC, some complexes were stable enough to sustain shearing forces caused by the HPLC separation matrix.

Finally, in comparison with αB_{WT}, the phospho-mimetic αB variant showed increased chaperone activity in aggregation assays (up to 2 times higher), as well as in refolding experiments (> 5 times higher) with the most basic refolding system (Hsc70 / Hdj1).

We conclude that, compared to the wild-type, phosphorylation of αB leads to an oligomeric species with amplified reactivity towards malate dehydrogenase at the conditions applied herein.

5.3 OUTLOOK

Future steps towards a better understanding of the chaperone function of αB-crystallin and its interconnections inside the chaperone network should include further optimization of the refolding system. Publications from other groups suggest the combination of the Hsc70 - Hdj1 - system with Bag1 (GrpE in *E.coli*) and / or a chaperonin system[55][18]. Additionally, replacement of Hdj1 by Hdj2 (another human homologue of the yeast J-domain protein) is worth a trial. To assure that ATPase activity is not limited by any side effect over the entire time span of up to 5 hours, an ATP regeneration system (comparable with the one applied in the ATPase assays presented herein) has been further employed [30].

In addition to that, the role of single phosphorylation sites would be interesting to uncover: are the effects presented herein originating from one sole phosphorylation site, or are they rather an accumulative result from all three phosphorylations? Phosphorylation of serin 45, for instance, has been linked to αB dimer disruption resulting in uncontrolled aggregation [51]. Therefore, one might consider exploring the effect of an αB variant phosphorylated at residues 19 and 59.

Moreover, to allow for a direct comparison with observations in literature, switching to a phospho-mimicking mutant containing serin to aspartate modifications instead of serin to glutamate would be helpful.

Besides experimental approaches, *in silico* experiments could bring further insight into the relation of the stability of oligomers and their decay into a broad distribution of multi-meric species. Molecular dynamics (MD) simulations would permit to imitate this process as subject to varied annealing scenarios. Additionally, the hypothesis of two αB occurrences - one that provides high substrate affinity as compared to a second with high substrate binding capacity - could be probed. Even though computational approaches are not yet regarded as daily business by experimental researches, MD has proven usefulness in many cases - either by offering rough, but powerful, coarse-grain models, or by providing detailed information that is not accessible by experiments [74][75][76][77].

Experimental ways to address the encountered polydispersity of the αB (- substrate) - system would comprise single-molecule (sm-) experiments, such as sm-FRET [78] or sm-force spectroscopy [77]. These approaches would allow to distinguish individual binding events or substrate affinities of distinct complexes, respectively.

ACKNOWLEDGMENTS

I thank my boyfriend Thomas Post for his support during this thesis work and ever since. Also my parents and my sisters I want to thank because they *assisted in folding* me into my actual form. Yet the freedom to choose my contacts, which they have always offered me, distinguishes them from a chaperone. Together with the *nano-family*, YOU enabled me to complete my major in nano-science.

Moreover, I thank Prof. Johannes Buchner for allowing me to accomplish this work in his laboratories and Prof. Markus Meuwly for supervising this thesis on behalf of the university of Basel.

My direct supervisor, Jirka Peschek, I thank for patiently teaching me all the protein chemical practice from scratch, and for his assistance throughout this thesis work in general.

Last but not at least, I want to thank the entire *Buchner Lehrstuhl* for the helping hands in the lab, as well as the friendly atmosphere surrounding the labs and the sympathetic ears you lent me.

BIBLIOGRAPHY

[1] Z. Xu, A. L. Horwich, P. B. Sigler, *Nature* **388**, 741 (1997).

[2] M. M. U. Ali, *et al.*, *Nature* **440**, 1013 (2006).

[3] S. Lee, M. E. Sowa, J.-M. Choi, F. T. F. Tsai, *Journal of Structural Biology* **146**, 99 (2004).

[4] B. Bösl, V. Grimminger, S. Walter, *Journal of Structural Biology* **156**, 139 (2006).

[5] H. S. Mchaourab, J. A. Godar, P. L. Stewart, *Biochemistry* **48**, 3828 (2009).

[6] M. Haslbeck, T. Franzmann, D. Weinfurtner, J. Buchner, *Nat Struct Mol Biol* **12**, 842 (2005).

[7] J. Peschek, *et al.*, *Proceedings of the National Academy of Sciences* **106**, 13272 (2009).

[8] J. ichi Ito, *Japanese PDB: 3C7N* (2009).

[9] J. P. Schuermann, *et al.*, *Molecular Cell* **31**, 232 (2008).

[10] L. Withmore, B. Wallace, *Biopolymers* **89**, 392 (2007).

[11] u. E. Wikipedia, Jablonski-schema — wikipedia, die freie enzyklopädie (2010). [Online; Stand 6. März 2010].

[12] u. S. J. Wikipedia, Förster-resonanzenergietransfer — wikipedia, die freie enzyklopädie (2010). [Online; Stand 6. März 2010].

[13] J. Lebowitz, M. S. Lewis, P. Schuck, *Protein Science* **11**, 2067 (2002).

[14] u. C. Wikipedia, Nicotinamide adenine dinucleotide — wikipedia, the free encyclopedia (2009). [Online; accessed 6-March-2010].

[15] T. U. Consortium, *Nucleic Acids Research* **36**, D190 (2008).

[16] J. C. Young, V. R. Agashe, K. Siegers, F. U. Hartl, *Nat Rev Mol Cell Biol* **5**, 781 (2004).

[17] S. Walter, J. Buchner, *Angewandte Chemie International Edition* **41**, 1098 (2002).

[18] A. P. Ben-Zvi, P. Goloubinoff, *Journal of Structural Biology* **135**, 84 (2001).

[19] B. DiDomenico, G. Bugaisky, S. Lindquist, *Proc Natl Acad Sci U S A* **79**, 6181 (1982).

[20] J. Chen, S. Walter, A. Horwich, D. Smith, *Nat Struct Biol* **8**, 721 (2001).

[21] S. K. Wandinger, K. Richter, J. Buchner, *Journal of Biological Chemistry* **283**, 18473 (2008).

[22] M. Mickler, M. Hessling, C. Ratzke, J. Buchner, T. Hugel, *Nat Struct Mol Biol* **16**, 281 (2009).

[23] Y. Chernoff, S. Lindquist, B. Ono, S. Inge-Vechtomov, S. Liebman, *Science* **268**, 880 (1995).

[24] L. Whitesell, S. L. Lindquist, *Nature Reviews Cancer* **5**, 761 (2005).

[25] H. Ecroyd, J. Carver, *Cellular and Molecular Life Sciences* **66**, 62 (2009).

[26] L. G. Goldfarb, M. C. Dalakas, *The Journal of Clinical Investigation* **119**, 1806 (2009).

[27] U. Jakob, J. Buchner, *Trends Biochem Sci.* **19**, 205 (1994).

[28] F. Bennardini, A. Wrzosek, M. Chiesi, *Circulation Research* **71**, 288 (1992).

[29] M. G. Santoro, *Biochemical Pharmacology* **59**, 55 (2000).

[30] G. J. Lee, E. Vierling, *PLANT PHYSIOLOGY* **122**, 189 (2000).

[31] M. Ehrnsperger, S. Graber, M. Gaestel, J. Buchner, *EMBO* **16**, 221 (1997).

[32] J. P. Brady, *et al.*, *Proceedings of the National Academy of Sciences* **94**, 884 (1997).

[33] S. Lee, D. J. Prochaska, F. Fang, S. R. Barnum, *Current Microbiology* **37**, 403 (1998).

[34] U. P. Andley, *Progress in Retinal and Eye Research* **26**, 78 (2007).

[35] H. Bloemendal, *et al.*, *Progress in Biophysics and Molecular Biology* **86**, 407 (2004).

[36] K. Kato, *et al.*, *Biochimica et Biophysica Acta (BBA) - General Subjects* **1074**, 201 (1991).

[37] M. F. Ahmad, B. Raman, T. Ramakrishna, C. M. Rao, *Journal of Molecular Biology* **375**, 1040 (2008).

[38] R. H. P. H. Smulders, W. W. de Jong, *FEBS Letters* **409**, 101 (1997).

[39] J. Horwitz, *et al.*, *Int J Biol Macromol.* **22**, 263 (1998).

[40] J. G. Ghosh, S. A. Houck, J. I. Clark, *The International Journal of Biochemistry & Cell Biology* **39**, 1804 (2007).

[41] F. Stengel, *et al.*, *Proceedings of the National Academy of Sciences* **107**, 2007 (2010).

[42] M. P. Bova, L.-L. Ding, J. Horwitz, B. K. K. Fung, *Journal of Biological Chemistry* **272**, 29511 (1997).

[43] R. Shashidharamurthy, H. A. Koteiche, J. Dong, H. S. Mchaourab, *Journal of Biological Chemistry* **280**, 5281 (2005).

[44] H. Yang, *et al.*, *Protein Sci.* **8**, 174 (1999).

[45] T. M. Franzmann, M. Wühr, K. Richter, S. Walter, J. Buchner, *Journal of Molecular Biology* **350**, 1083 (2005).

[46] J. A. Aquilina, *et al.*, *Journal of Biological Chemistry* **280**, 14485 (2005).

[47] Z. MA, *et al.*, *Experimental Eye Research* **67**, 21 (1998).

[48] H. Ito, K. Okamoto, H. Nakayama, T. Isobe, K. Kato, *Journal of Biological Chemistry* **272**, 29934 (1997).

[49] H. A. Koteiche, H. S. Mchaourab, *Journal of Biological Chemistry* **278**, 10361 (2003).

[50] H. Ito, *et al.*, *Journal of Biological Chemistry* **276**, 5346 (2001).

[51] J. A. Aquilina, *et al.*, *Journal of Biological Chemistry* **279**, 28675 (2004).

[52] J. den Engelsman, *et al.*, *Eur J Biochem.* **271**, 4195 (2004).

[53] J. den Engelsman, *et al.*, *Journal of Biological Chemistry* **280**, 37139 (2005).

[54] K. Kato, *et al.*, *J Neurochem.* **76**, 730 (2001).

[55] A. Mogk, *et al.*, *Journal of Biological Chemistry* **278**, 31033 (2003).

[56] H. Inoue, H. Nojima, H. Okayama, *Gene* **96**, 23 (1990).

[57] M. Gething, J. Sambrook, *Nature* **300**, 598 (1982).

[58] S. P. Fling, D. S. Gregerson, *Analytical Biochemistry* **155**, 83 (1986).

[59] G. Fairbanks, T. L. Steck, D. Wallach, *Biochemistry* **10**, 2606 (1971).

[60] J. T. Pelton, L. R. McLean, *Analytical Biochemistry* **277**, 167 (2000).

[61] A. Beer, *Annalen der Physik* **86**, 78 (1852).

[62] E. Gasteiger, *et al.*, *The Proteomics Protocols Handbook* pp. 571–607 (2005).

[63] J. R. Lakowicz, *Springer, New York* pp. 3–5 (2006).

[64] J. R. Lakowicz, *Springer, New York* p. 444 (2006).

[65] J. R. Lakowicz, *Springer, New York* pp. 448–449 (2006).

[66] P. Schuck, *Biophysical Journal* **78**, 1606 (2000).

[67] T. L. Tapleya, T. M. Franzmann, S. Chakrabortyb, U. Jakoba, J. C. Bardwell, *PNAS* **107**, 1071 (2010).

[68] J. Norb, *Methods in Enzymology* **156**, 116 (1988).

[69] G. L. Ellman, *Archives of Biochemistry and Biophysics* **82**, 70 (1959).

[70] C. Riener, G. Kada, H. Gruber, *Anal Bioanal Chem* **373**, 266 (2002).

[71] BRENDA, *Entry 1.1.1.37 - malate dehydrogenase* (2010).

[72] S. Sadis, L. E. Hightower, *Biochemistry* **31**, 9406 (1992).

[73] K. P. Das, W. K. Surewicz, *FEBS Letters* **369**, 321 (1995).

[74] J. Zhang, *et al.*, *IUBMB Life* **61**, 627 (2009).

[75] R. D. Schaeffer, A. Fersht, V. Daggett, *Current Opinion in Structural Biology* **18**, 4 (2008).

[76] S. A. Adcock, J. A. McCammon, *Chemical Reviews* **106**, 1589 (2006).

[77] M. Sotomayor, K. Schulten, *Science* **316**, 1144 (2007).

[78] X. Michalet, S. Weiss, M. Jäger, *Chemical Reviews* **106**, 1785 (2006).

DECLARATION

I declare that the thesis hereby submitted is my own original work. It has neither been published, nor been presented as examination material before. I affirm further that I cite my references to the best of my knowledge.

München, April 2010

Sonja Schmid

A

APPENDIX

A.1 PCR-PRIMERS

for: forward, rev: reverse, restr. site: restriction site.

Name:	Sequence:	Restr. site:
αB_{WT} for:	5′ - GATCCCATGGACATCGCCATCCACCACC - 3′	NcoI
αB_{WT} rev:	5′ - GATCGCGGCCGCCTATTTCTTGGGGGCTGC - 3′	NotI
αB-A4C for:	5′ - GATCCCATGGACATCTGCATCCACCACCC - 3′	NcoI
αB-S19E for:	5′ - CTTCTTTCCTTTCCACGAGCCCAGCCGCCTCTTTG - 3′	
αB-S19E rev:	5′ - CAAAGAGGCGGCTGGGCTCGTGGAAAGGAAAGAAG - 3′	
αB-S45E for:	5′ - GACGTCTACTTCCCTGGAGCCCTTCTACCTTCG - 3′	
αB-S45E rev:	5′ - CGAAGGTAGAAGGGCTCCAGGGAAGTAGACGTC - 3′	
αB-S59E for:	5′ - CTTCCTGCGGGCACCCGAGTGGTTTGACACTGG - 3′	
αB-S59E rev:	5′ - CCAGTGTCAAACCACTCGGGTGCCCGCAGGAAG - 3′	

A.2 AGAROSE GELS

The standard in the agarose gels displayed below includes the following kilo base numbers: 0.5, 1, 1.5, 2, 3, 4, 5, 6, 8, 10 kb.

Incorporation of the second mutation. The PCR worked only for the forward constructs, i.e. every second lane in the gel below:

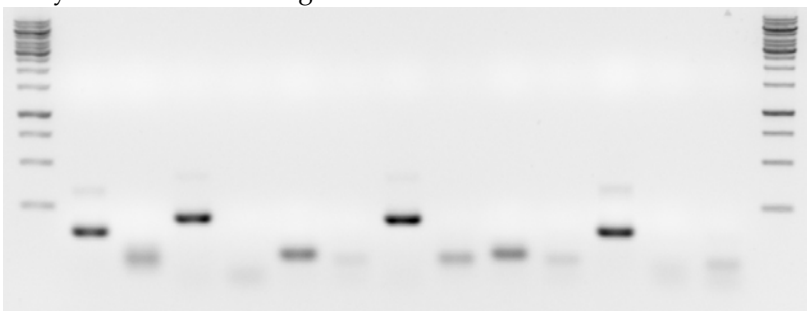

Backwards constructs were obtained with a newly bought primer:

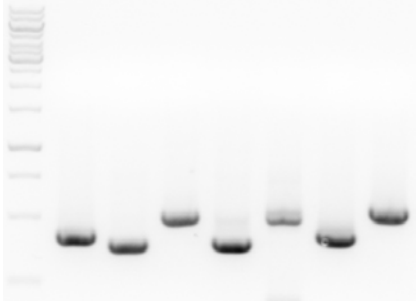

Linker PCR of the double and triple mutants and a control. Because of the double bands, the constructs were excised from the gel:

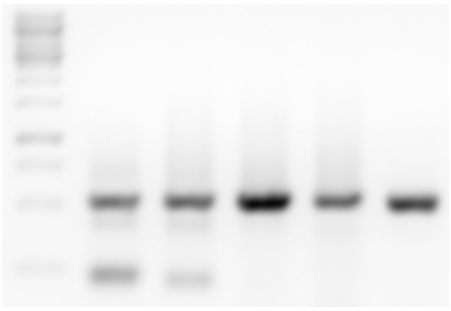

Incorporation of the additional cystein at residue 4 of the 3E-mutant:

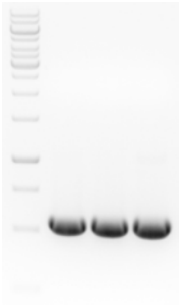

A.3 PURIFICATION CHROMATOGRAMS & SDS-GELS

A.3.1 *Purification of* αB_{WT}

Chromatograms were presented in the report. In the following the corresponding gels are displayed:

Result of *Q-Sepharose* column:

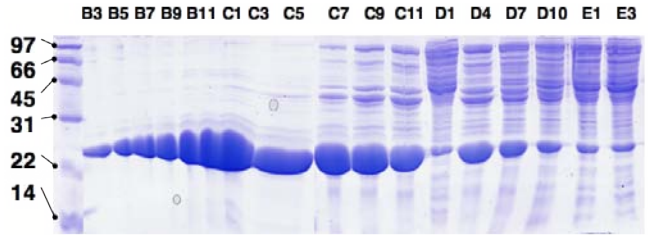

Result of *Superdex 200*:

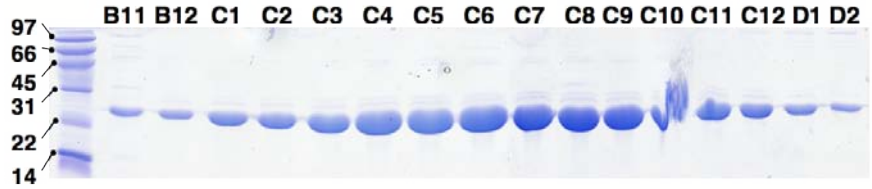

Result of *Resource Q*:

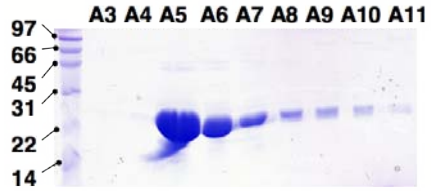

A.3.2 *Purification of αB-3E*

The molecular weight standard is the same as before.

Q-Sepharose:

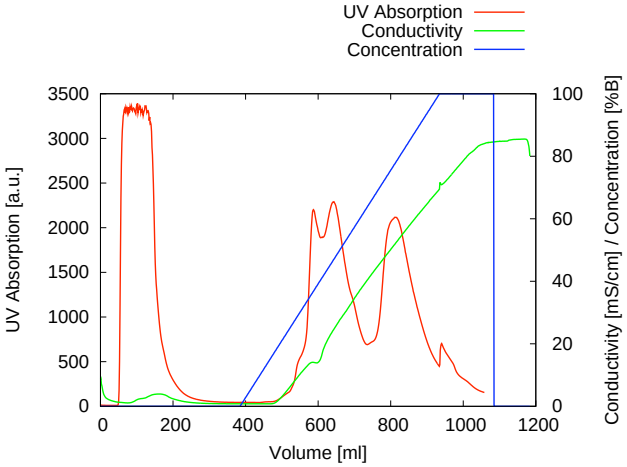

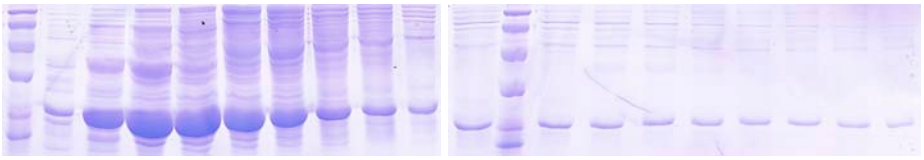

Superdex 200:

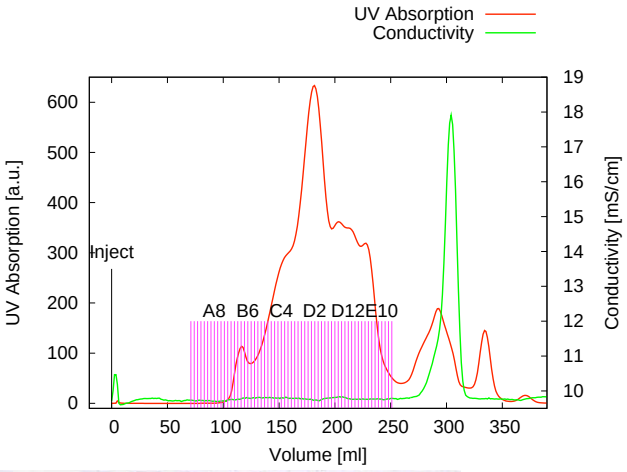

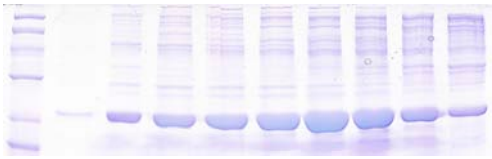

Resource:

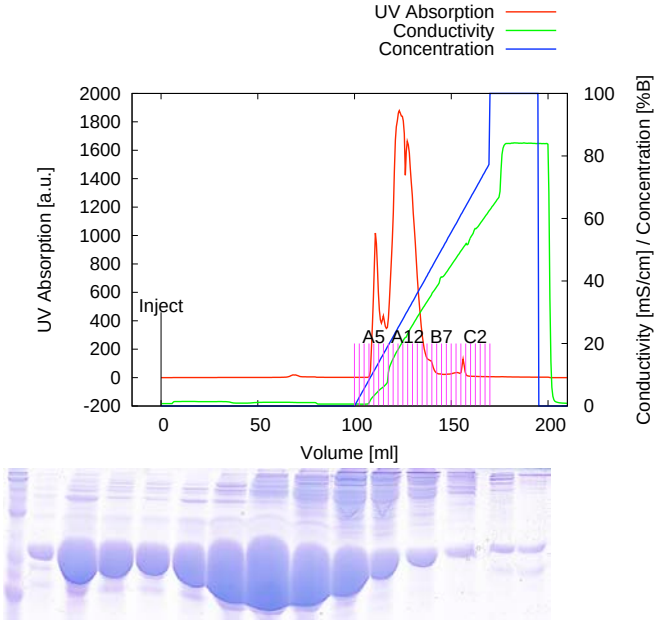

A.3.3 *Purification of αB-A4C-3E*

Q-Sepharose:

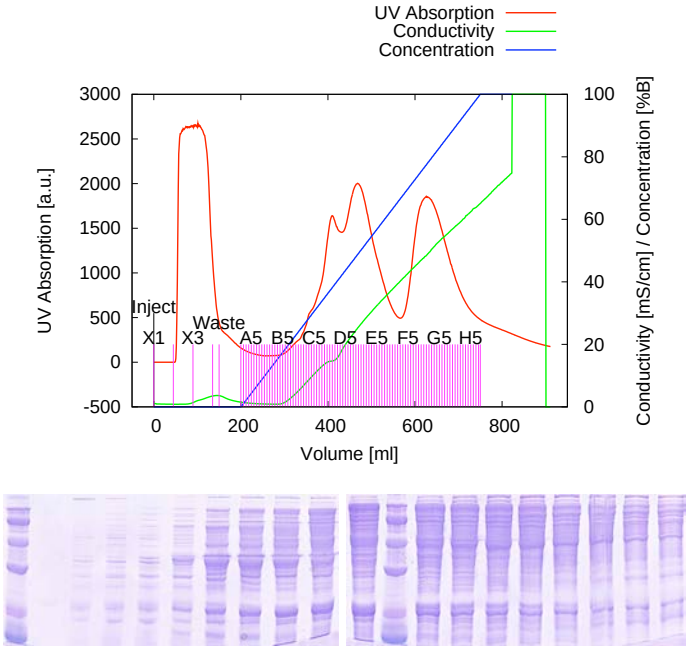

Superdex 200:

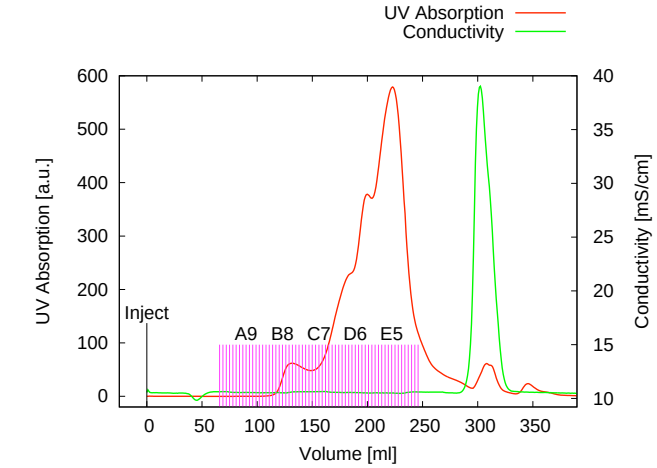

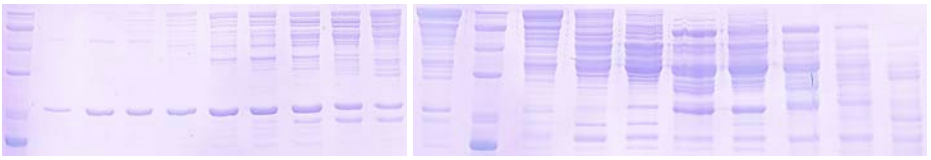

Resource:

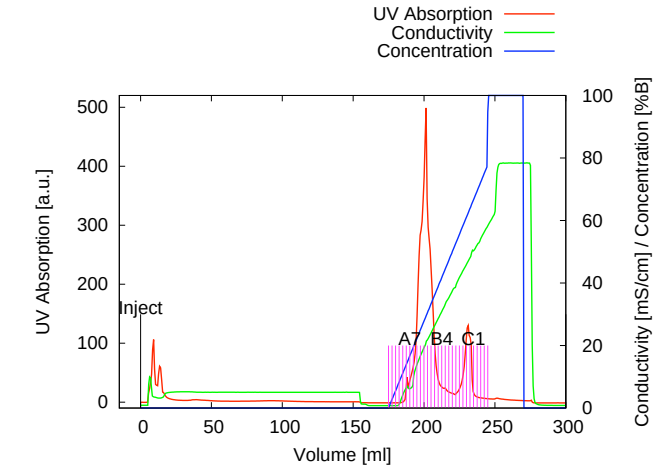

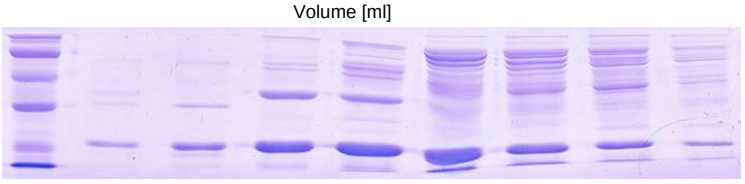

COLOPHON

This thesis was typeset with LaTeX 2ε using André Miede's *classicthesis* package. The typographic style was inspired by Robert Bringhurst's *The Elements of Typographic Style*.

Final Version as of April 20, 2010 at 14:36.